Methanol Synthesis

K. KLIER

Department of Chemistry and Center for Surface and Coatings Research
Lehigh University
Bethlehem, Pennsylvania

I. Introduction 243
II. Catalyst Selection 251
III. The Activity of Pure Copper Metal 254
IV. The Activity of Pure Zinc Oxide 257
V. The Binary Copper–Zinc Oxide System 257
A. Preparation of the Cu/ZnO Binary Catalysts 258
B. Physical Characteristics of the Cu/ZnO Catalysts 258
C. Particle Size and Morphology 261
D. Surface Analysis by XPS–Auger Spectroscopy 266
E. Surface Areas of the Individual Catalyst Components 267
F. Chemisorption of Carbon Monoxide and Hydrogen 268
G. Activity Patterns 271
H. Reaction Kinetics in the Presence of Carbon Dioxide 274
I. The Effect of Carbon Dioxide on Selectivity 284
J. Relative Hydrogenation Rates of Carbon Monoxide, Hydrocarbons, and Oxygenates 285
VI. Other Binary Catalysts 287
A. Copper-Based Catalysts 287
B. Transition-Metal-Based Catalysts 289
VII. Ternary and Quaternary Catalysts 291
VIII. Mechanisms 296
A. Possible Reaction Pathways 297
B. Methods Used in Mechanistic Studies of Methanol Synthesis . . 299
C. Evidence for Adsorbed Carbon Monoxide and Hydrogen 302
D. Evidence for Adsorbed Formate and Methoxide 303
E. Surface Complexes Formed by Coadsorption of the Reactants . . 304
F. Mechanism of Methanol Synthesis at Low Temperatures and Pressures 308
References 310

I. Introduction

Methanol synthesis is a process of major industrial importance consisting of hydrogenation of carbon monoxide or of carbon dioxide according to the equations

$$CO + 2H_2 \rightleftharpoons CH_3OH \quad (1)$$

Copyright © 1982 by Academic Press, Inc.
All rights of reproduction in any form reserved.
ISBN 0-12-007831-7

where $\Delta H_{600K} = -100.46$ kJ/mol and $\Delta G_{600K} = +45.36$ kJ/mol;

$$CO_2 + 3H_2 \rightleftharpoons CH_3OH + H_2O \tag{2}$$

where $\Delta H_{600K} = -61.59$ kJ/mol and $\Delta G_{600K} = +61.80$ kJ/mol. Methyl alcohol is one of the least thermodynamically probable products of CO and CO_2 hydrogenations, since the formation of higher alcohols and hydrocarbons is accompanied with more negative free-energy change, as illustrated in Fig. 1. Dimethylether (DME) may also be produced by the dehydration

$$2CH_3OH \rightleftharpoons CH_3OCH_3 + H_2O \tag{3}$$

where $\Delta H_{600K} = -20.59$ kJ/mol and $\Delta G_{600K} = -10.71$ kJ/mol.

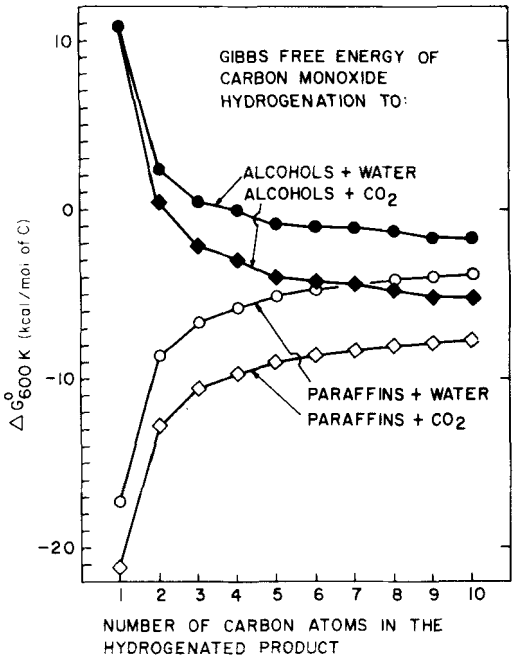

FIG. 1. Gibbs free energies ΔG° at 600 K (kcal/mol of carbon) in the product alcohol or hydrocarbon of the reactions:

$$n\text{CO} + 2n\text{H}_2 \rightarrow \text{CH}_3(\text{CH}_2)_{n-1}\text{OH} + (n-1)\text{H}_2\text{O} \quad (\bullet)$$
$$(2n-1)\text{CO} + (n+1)\text{H}_2 \rightarrow \text{CH}_3(\text{CH}_2)_{n-1}\text{OH} + (n-1)\text{CO}_2 \quad (\blacklozenge)$$
$$n\text{CO} + (2n+1)\text{H}_2 \rightarrow \text{CH}_3(\text{CH}_2)_{n-2}\text{CH}_3 + n\text{H}_2\text{O} \quad (\circ)$$
$$2n\text{CO} + (n+1)\text{H}_2 \rightarrow \text{CH}_3(\text{CH}_2)_{n-2}\text{CH}_3 + n\text{CO}_2 \quad (\diamond)$$

From D. R. Stull, E. F. Westrum, and G. C. Sinke, "The Chemical Thermodynamics of Organic Compounds." Wiley, New York, 1969. 1 cal = 4.184 J.

To avoid the formation of DME, higher alcohols, and hydrocarbons, methanol synthesis requires a selective catalyst that rapidly executes the hydrogenation of CO or CO_2 to methyl alcohol but at the same time does not allow the reaction to proceed any further downhill on the thermodynamic free-energy scale. Based on general experience with catalysts in other hydrogenation reactions, this would appear a formidable if not an impossible task. However, after the development involving some six decades, industry now does have a catalyst which selectively steers the hydrogenation of the synthesis gas, $CO + CO_2 + H_2$ in various proportions, to almost pure methanol. The activity, and consequently, the pressure and temperature range at which the methanol synthesis catalysts operate have undergone dramatic changes in the last two decades, which culminated in the commercialization of the so-called low-pressure process operating at pressures less than 100 atm. The low-pressure catalysts invariably contain copper and a mixture of oxides such as $ZnO–Al_2O_3$ or $ZnO–Cr_2O_3$. Oxides V_2O_5, V_2O_3, ThO_2, and others have also been claimed as effective components of the low-pressure copper-based catalysts.

The credit for the first invention of the copper-based catalysts goes to M. Patart (*1*), who has patented many inorganic oxides, salts, and metals, including copper, for methanol synthesis at pressures 150–200 atm and temperatures 300–600°C. Following Patart's work, several investigators noted the curious fact that oxides and copper separately had relatively low activity, whereas mixtures of an oxide and copper increased the yield considerably. It was this mutual promotion effect to which many conflicting reports on the activity of copper-based catalysts could be traced. Realization came early that preparation of copper catalysts is an extremely important factor in determining their activity for methanol. In one report, copper catalysts prepared by precipitation by alkali hydroxide were active, while those precipitated by ammonium hydroxide were inactive, and suspicion was raised that alkaline impurities may be responsible for the activity of copper catalysts (*2*). Methanol decomposition also gave conflicting results in the early research. Sabatier and co-workers, who first employed methanol decomposition as a guide for finding active methanol synthesis catalysts, found many catalysts, including copper, that decomposed methanol (*3*, *4*), but the attempts to synthesize methanol by the reverse process gave very poor results with copper catalysts (*5*). The question of the activity of copper and of the promotion effect of zinc oxide was further investigated by Frolich and his co-workers (*6*, *7*), who prepared the whole range of binary compositions CuO/ZnO from 0/100 to 100/0 by coprecipitation of hydroxides from nitrate solutions by ammonia, calcination at 220°C, and reduction by methanol at 200–220°C. The key results of their methanol decomposition

(*6*) and methanol synthesis (*7*) study are summarized in Fig. 2. At 360°C and 204 atm, zinc oxide was quite a good catalyst for both the decomposition and the synthesis, while copper, which was present in the form of metal, as Frolich *et al.* showed later (*8*), displayed some activity for the decomposition but none for the synthesis. The maximum rate of the synthesis and decomposition reactions appeared at catalyst compositions near CuO/ZnO = 30/70, and Frolich *et al.* (*8*) engaged in a study to elucidate the nature of this

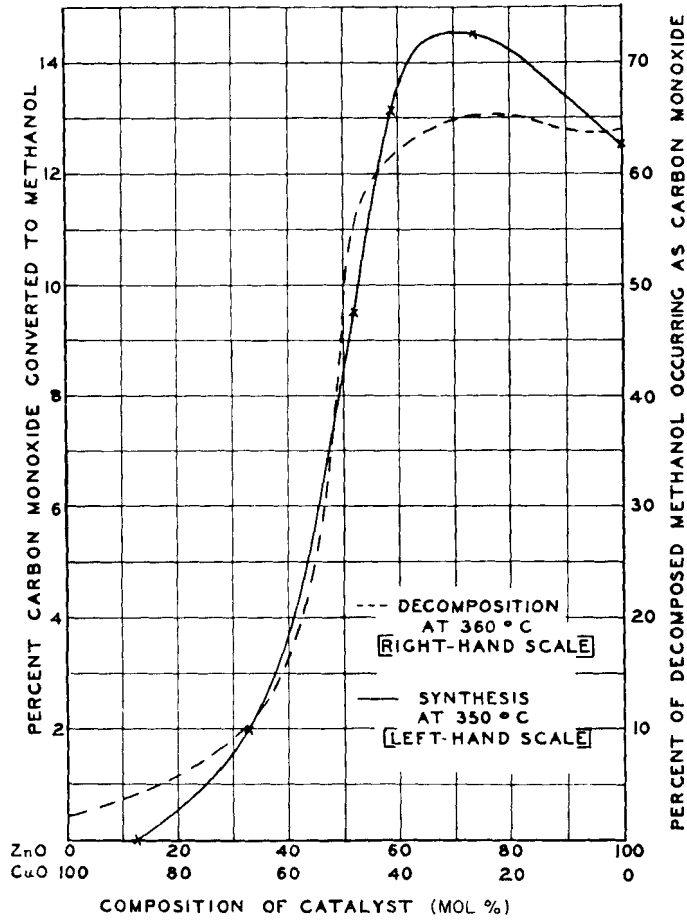

FIG. 2. Comparison of methanol decomposition at 360°C and atmospheric pressure with synthesis at 350°C and 204 atm using the same catalysts (*7*). [Reprinted with permission from *Ind. Eng. Chem.* **20,** 1327 (1928). Copyright (1928) American Chemical Society.]

effect by X-ray determinations of the lattice constants of copper and zinc oxide over the whole compositional range.

Indeed, lattice parameters of both the copper and the zinc oxide were found to depend on the catalyst composition. The lattice extension of copper was attributed to alpha brass formation upon partial reduction of zine oxide, and an attempt was made to correlate the lattice constant of copper with the decomposition rate of methanol to methyl formate. Furthermore, the decomposition rate of methanol to carbon monoxide was found to correlate with the changes of lattice constant of zinc oxide. Although such correlations did not establish the cause of the promotion in the absence of surface-area measurements and of correlations of specific activities, the changes of lattice parameters determined by Frolich *et al.* are real and indicate for the first time that the interaction of catalyst components can result in observable changes of bulk properties of the individual phases. Frolich *et al.* did not offer an interpretation of the observed changes in lattice parameters of zinc oxide. Yet these changes accompany the formation of an active catalyst, and much of this review will be devoted to the origin, physicochemical nature, and catalytic activity of the active phase in the zinc oxide–copper catalysts.

The patterns of methanol decomposition rates were qualitatively confirmed by Kostelitz and Hüttig (*9*) who concluded in an extensive study of the whole Cu/ZnO compositional range that a "synergic promotion" took place in the zinc-oxide-rich catalysts which also displayed the highest activity. The term synergic promotion was coined by Mittasch to describe effects due to chemical and physical interactions of the catalyst components, as opposed to "structural promotion," associated with increasing or maintaining the surface area of the active substance without changing the activity of unit area. The synergic promotion was described by Kostelitz and Hüttig in the following words: "Es müssen sich also an den Kupfer-Zinkoxyd-Phasengrenzflächen spezifisch wirkende Kraftfelder herausgebilt haben, denen ein wesentlicher Anteil an der katalytischen Wirksamkeit zugeschrieben werden muss," i.e., "There must be specifically acting force fields built up at the copper–zinc oxide interfaces, to which a substantial part of the catalytic activity must be attributed." The thread of evidence and thought that an active catalyst is formed by the coexistence and through the physicochemical interactions of two or more separate solid-phase components, has once again appeared in the early catalytic literature. With the experimental tools of the first half of the century, however, it was not possible to analyze what the "spezifisch wirkende Kraftfelder" were and how they were related to catalysis.

It must be noted that despite these interesting findings and interpretative

developments, it was not demonstrated until much later that the copper–zinc oxide catalysts would work at low pressures, and industry used instead a catalyst based on zinc oxide and chromia (also termed "zinc chromite") in a high-pressure process commercialized by BASF in 1923 (*5*). As late as 1955, the copper–zinc oxide–chromia catalyst was considered by Natta as impractical because of its poor resistance to thermal shocks, concomitant poor reproducibility, and sensitivity to chemical poisons (*10*).

The development of the high-pressure process, which included thorough kinetic studies, was reviewed by Natta (*10*). In the 1950s methanol synthesis appeared to be a mature process and zinc chromite a very satisfactory catalyst. The decade of 1960s brought a dramatic industrial breakthrough, however. Pioneered by ICI, soon followed by other companies, low-pressure methanol synthesis processes emerged, all utilizing ternary catalysts based on copper, zinc oxide, and another oxide such as chromia or alumina. Although the basic combination copper–zinc oxide had been known to be an active methanol synthesis catalyst for a considerable length of time, it was the more systematic and careful, although apparently still quite empirical, preparation and testing of the mixed catalysts that led to the new process in which the synthesis was carried out at pressures of 50–100 atm and temperatures of 220–250°C. Tables I and II summarize catalyst compositions, conditions, and methanol yields for these various new low-pressure catalysts. Compared to the older high-pressure processes which ran typically at 200 atm and 350°C, the low-pressure conditions offered such economic and operational advantages that virtually all the world's methanol plants built after 1967 were the low-pressure plants.

Along with the commercial success of the new low-pressure process, there emerged a renewed research activity aiming at the scientific understanding of the function of the copper-containing mixed-oxide catalysts. Furthermore, various reports summarized in a recent review by Denny and Whan (*26*) indicated that carbon dioxide has a significant effect on the synthesis rates, and Andrew recently reported (*27*) that the dependence of the synthesis rate on carbon dioxide concentration has a maximum around 1% CO_2, a result derived from tests involving the commercial ICI catalyst $Cu/ZnO/Al_2O_3$.

It appears probable, and will be substantiated below, that the effects of CO_2 and the "synergic promotion" of one catalyst component by another are but two facets of the formation of an active catalyst through the interactions among its components and the surrounding gas phase. It is the purpose of this article to review the recent observations and interpretations concerning the distribution of phases and elements, the physicochemical state of the catalyst components, the mode of activation of the reactants, and to show that a consistent picture is emerging that elucidates the function of the copper-based catalysts in the synthesis mechanism.

TABLE I

Cu/Zn/Al Oxide Catalysts Used in the Synthesis of Methanol

Composition[a] (wt. %)	Reactants[b]	Temp. (°C)	Pressure (atm)	Space velocity (hr^{-1})	Yield (kg $liter^{-1}$ hr^{-1})	Company	Reference
12:62:25	2	230	200	10,000	3.290	BASF	*11*
	2	230	100	10,000	2.086	BASF	
23:46:30	3	240		20,000	2.5	CCI	*12*
24:38:38	2	226	50	12,000	0.7	ICI	*13*
35:45:20	1	250				Academic	*14*
53:27:6	1	250	50			ICI	*15*
60:22:8	1	250	50	40,000	0.5	ICI	*16*
	2	226	100	9600	0.5	ICI	
64:32:4	3	250	50	10,000	0.3	Academic	*17*
	3	300	50	10,000	0.9	Academic	
66:17:17	1	275	70	200[d]	4.75	DuPont	*18*
c	1	250	50	10,000		Academic	*19*

[a] $CuO:ZnO:Al_2O_3$.

[b] 1, $H_2 + CO + CO_2$; 2, $H_2 + CO + CO_2 + CH_4$; 3, $CO + H_2$; N_2 is sometimes used as a diluent.

[c] SNM-1 catalyst.

[d] Moles per hour.

TABLE II

Cu/Zn/Cr Oxide Catalysts Used in the Synthesis of Methanol

Composition[a] (wt. %)	Reactants[b]	Temp. (°C)	Pressure (atm)	Space velocity (hr^{-1})	Yield (kg $liter^{-1}$ hr^{-1})	Company	Reference
11:70:19	3	250		4000		Power-Gas Corp.	*20*
15:48:37	3	270	145	10,000	1.95[c]	Jap. Gas-Chem. Co.	*21*
31:38:5	3	230	50	10,000	0.755	BASF	*22*
	4	230	50	10,000	1.275	BASF	
33:31:36	3	250	150	10,000	1.1	Academic	*17*
	3	300	150	10,000	2.2	Academic	
40:10:50	1	260	100	10,000	0.48[c]	T, HFA	*23*
40:40:20	2	250	40	6000	0.26	ICI	*24*
	2	250	80	10,000	0.77	ICI	
60:30:10	1	250	100	9800	2.28	Metall-Gesellschaft	*25*

[a] $CuO:ZnO:Cr_2O_3$.

[b] 1, $H_2 + CO + CO_2$; 2, $H_2 + CO + CO_2 + CH_4$; 3, $CO + H_2$; 4, $CO + H_2 + O_2$; N_2 is sometimes used as a diluent.

[c] Kilograms per kilogram per hour.

II. Catalyst Selection

Methanol synthesis from carbon monoxide formally consists of an attachment of three hydrogen atoms onto the carbon end and of one hydrogen atom onto the oxygen end of the CO molecule without the cleavage of the carbon–oxygen bond. The two bonding π orbitals of carbon monoxide, the lone pair (5σ) orbital or carbon, and the σ orbitals of two hydrogen molecules are utilized to make three C—H sigma bonds, one O—H sigma bond, and one additional lone pair orbital on the oxygen atom, schematically.

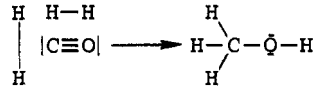

The carbon–oxygen sigma (3σ) and the lone-pair oxygen (4σ) orbitals remain intact except for a change in electron repulsion.

These features of the reaction impose the following requirements on the catalyst:

1. The catalyst must not cleave the carbon–oxygen sigma bond ($\sim$360 kJ/mol).
2. The catalyst must activate carbon monoxide molecule so that hydrogenation can occur on both ends of the molecule.
3. The catalyst must be a fairly good hydrogenation catalyst which activates hydrogen molecules in a manner suitable for the above reaction. From the pattern of bonds broken and formed, this appears to require splitting of hydrogen molecules on the catalyst surface at some stage of the reaction.

Although all three requirements must be satisfied by a good methanol catalyst, there is evidence that activation of carbon monoxide is more difficult than that of hydrogen. It is therefore instructive first to examine the ability of various catalysts to activate CO by nondissociative chemisorption.

For metals there exists a clear-cut relationship between their position in the periodic table and their ability to chemisorb CO dissociatively. A division line has been established for ambient temperature by Brodén *et al.* (*28*) between metals that chemisorb CO nondissociatively and those which have at least some crystal faces that split the CO molecule into surface carbon and oxygen. Table III shows a section of the periodic table wherein elements on the right-hand side of the borderline adsorb CO nondissociatively and vice versa. Brodén *et al.* have also demonstrated on the basis of UV photoelectron spectroscopic measurements that the π–4σ energy separation is affected by the bonding of undissociated carbon monoxide to the metal surface: the (π–4σ) energy gap increases with increasing strength of the carbon-to-metal

TABLE III
CO Chemisorption on Transition Metals[a]

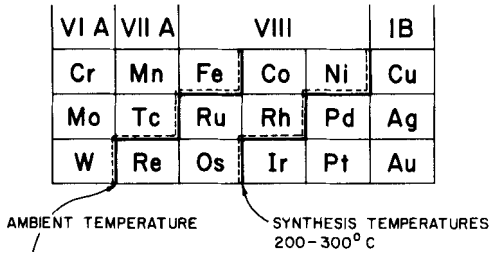

[a] Dividing lines separate metals on the left which split CO from those on the right which adsorb CO nondissociatively.
[b] Brodén *et al.* (1976).

bond as is apparent from Table IV. The differences of the $(\pi-4\sigma)$ energy gap for metals on the two sides of the room-temperature borderline are only tenths of electron volt (10 kJ) however, and it is entirely expectable that the borderline will depend on temperature. At high temperatures, cracking of carbon monoxide will become more probable, and so the borderline will move to the right. Although no measurements similar to those by Brodén *et al.* have been reported for elevated temperatures, the chemical behavior of various metal catalysts permits the conclusion that the division line between nondissociative and dissociative CO chemisorption lies, at 250–300°C, between nickel and copper, rhodium and palladium, and osmium and iridium. This high-temperature division line is also indicated in Table III. At still higher temperatures, even copper and palladium will dissociate carbon monoxide.

It must be emphasized that nondissociative chemisorption of carbon monoxide, which appears to be a necessary condition for its hydrogenation to methanol, is not a *sufficient* prerequisite. For example, nickel (*29*) or gold

TABLE IV
Weakening of the C—O Bond by Back-Donation Metal → CO $(2\pi^*)$[a]

Mo, Fe	>	W	>	Ru	>	Ni	>	Pd	>	Ir	>	Pt
3.50		3.20		3.15		3.08		2.90		2.75		2.60

[a] Consequences: $E(1\pi)$ increases more than $E(4\sigma)$ and $\Delta(1\pi-4\sigma)$ increases with back-bonding. The average values of Δ for different transition metals are in electron volts. The scatter of Δ for different crystal faces is 0.2 eV (0.026 eV = 300 K). From Ref. *28*.

(*30*) chemisorb CO nondissociatively at ambient temperature but they are not methanol synthesis catalysts. Of the metals on the right-hand side of the high-temperature borderline in Table III, copper (*31*), palladium, platinum, and iridium (*32*) have been reported to be selective methanol synthesis catalysts, while certain forms of rhodium have been found catalysts of intermediate activity and selectivity for methanol (*33*, *34*). All these metals have the common property that they lie close to the high-temperature borderline in Table III. Moreover, metals guiding the synthesis selectively to methanol are to the right, but not far to the right, of this boundary. This indicates that good methanol catalysts chemisorb CO with moderate strength, which is sufficient to perturb this molecule to enable it to react with hydrogen but insufficient to break it or any of the intermediates into fragments.

Aside from depending on the position of the metal in the periodic table as outlined above, the catalytic activity of each individual metal further depends on its physical and chemical state. Therefore, while the nondissociative chemisorption of CO serves as a crude guiding principle for the selection of a catalyst that will *potentially* synthesize methanol, the optimum performance of the catalyst results from maximizing and stabilizing its form that is most active, and in the case of methanol also most selective, under the desired reaction conditions. Factors that have contributed to the development of the low-pressure methanol catalyst have been the stability of metal dispersion; the choice of oxide "support"; the concentration of impurities such as alkali-, sulfur-, and chlorine-containing compounds; preparation variables giving rise to different precursor compounds; calcination and reduction regimes; etc. After a complex preparation procedure, pinpointing the "active form" of a catalyst appears to be a difficult task. Experimental efforts to find the active component of a given catalyst often spur controversies, and the history of the copper-based methanol catalyst is a prime example of a collection of "puzzling results," claims and denials, and disagreements among the various workers in the field. The early investigations dating back to Sabatier, Patart, Frolich, and Hüttig were outlined in Section I. After the successful development of the low-pressure process, debate has concentrated on the active component of the $Cu/ZnO/Al_2O_3$ catalyst. Detailed description and analysis of this system are offered in the following text. The palladium, platinum, iridium, and rhodium catalysts have not been considered as of this writing for commercial applications because their activity was found to be significantly lower than that of the modern copper-based catalysts.

While the relation between the position of *metals* in the periodic table and their ability to synthesize methanol has been established, a similar pattern is lacking for *oxides* (*35*). It can be anticipated that the requirements 1–3, listed earlier, must also be satisfied by oxide catalysts, but so far attempts

have not been made to link the methanol-synthesis activity of oxides with their physicochemical properties such as basicity or acidity, metal–oxygen bond strength, energy gap and semiconductivity, work function and electron affinity, etc. There does appear to be consensus among the workers in the field that surface acidity of an oxide leads to the formation of dimethyl ether by a reaction consecutive to methanol synthesis.

III. The Activity of Pure Copper Metal

The early conflicting reports on the activity of pure copper metal could not be reconciled without the simultaneous or concurrent measurements of activity, surface area, and surface composition. Moreover, it became evident that it is important to use unsupported copper as the reference material to avoid support–metal interactions that may influence the catalytic properties of the latter.

In order to resolve the issue of the activity of pure copper metal, the following experiment has been carried out in the author's laboratory (*36*): Copper hydroxy nitrate [$Cu_2(OH)_3NO_3$] was precipitated from a solution of copper nitrate by a dropwise addition of sodium carbonate, carefully washed and stepwise calcined at temperatures not exceeding 350°C. X-ray diffraction showed the product of calcination to be crystalline CuO (tenorite) and Auger surface analysis was able to detect only copper and oxygen. Careful search for Na, N, Fe, Cl, and S revealed that these elements were absent to within the detection limits of the technique, i.e., 0.02–1 at. % on the surface. The CuO catalyst was then loaded into a reactor in which many active catalysts were tested, reduced in a stream of 2% H_2 in N_2 at atmospheric pressure and 250°C, and subject to a standard methanol synthesis test by passing the synthesis gas $CO/CO_2/H_2 = 24/6/70$ at 75 atm and 250°C at the rate 15 liters (STP)/hr over 16 g of the copper catalyst. The effluent was analyzed by an on-line gas chromatograph, and the carbon conversion to methanol was found to be less than 0.001% under the outlined conditions. No dimethyl ether was detected. However, small amounts of water (0.005%) and methane (0.036%) were found in the effluent gas. The catalyst was removed under nitrogen and subjected to X-ray diffraction, BET surface area measurement, and Auger analysis. X-ray diffraction determined copper to be in its normal fcc crystalline state with the cubic lattice constant that of bulk copper metal (*36*). The BET surface area was found to be 0.43 m^2/g, so that the 16 g of the tested catalyst exposed an area of 6.88 m^2 to the synthesis gas. A scanning electron micrograph of this copper specimen is shown in Fig. 3. The analysis of argon isotherms indicated that the metal was not

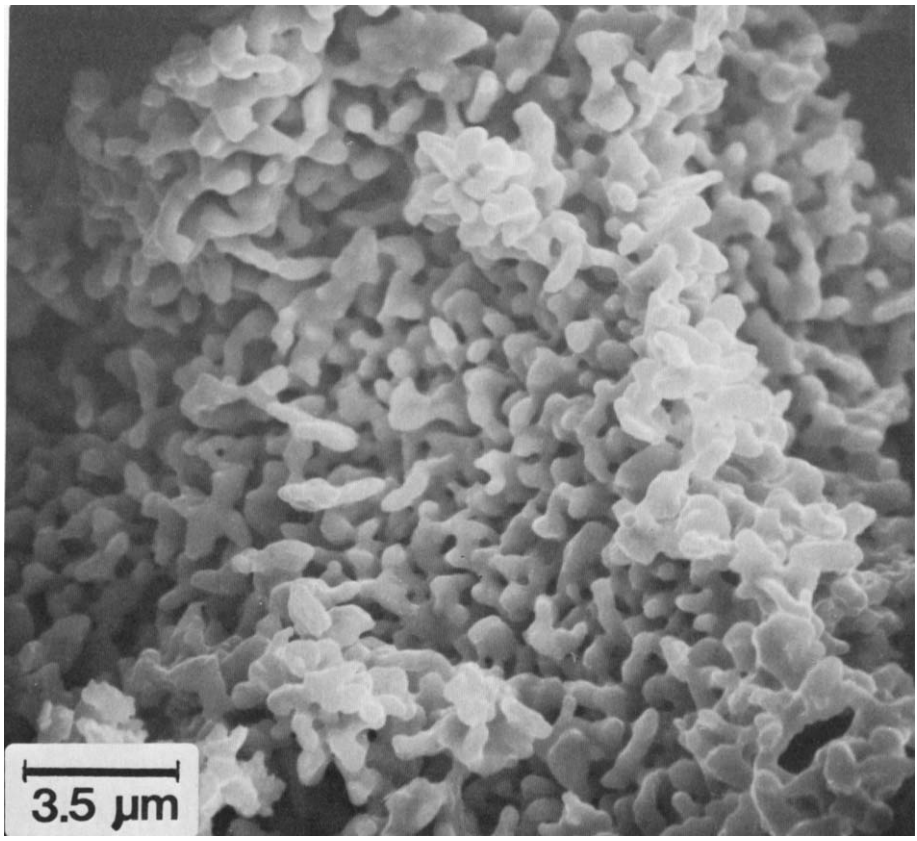

FIG. 3. Scanning electron micrograph of copper used in methanol synthesis study (*40*). [Reprinted with permission from *J. Catal.* **57,** 339 (1979). Copyright (1979) Academic Press, New York.]

microporous (*37*). A sample of the used copper catalyst was subject, after a brief exposure to air, to Auger analysis, which found no other elements than copper and oxygen on the catalyst surface. The catalyst was then reduced in the Auger spectrometer at 250°C, and only copper was found in its surface.

This set of experiments establishes that pure copper metal, free of surface impurities, yields less than 10^{-8} kg of methanol per square meter of the catalyst per hour under the standard conditions outlined above. Such a yield is far below the specific activity of "supported" copper-based catalysts, e.g., 3.63×10^{-5} kg CH_3OH m^{-2} hr^{-1} for the Cu/ZnO = 30/70 catalyst (*39*), and shows that copper metal is a very poor catalyst for methanol synthesis at 75 atm at 250°C.

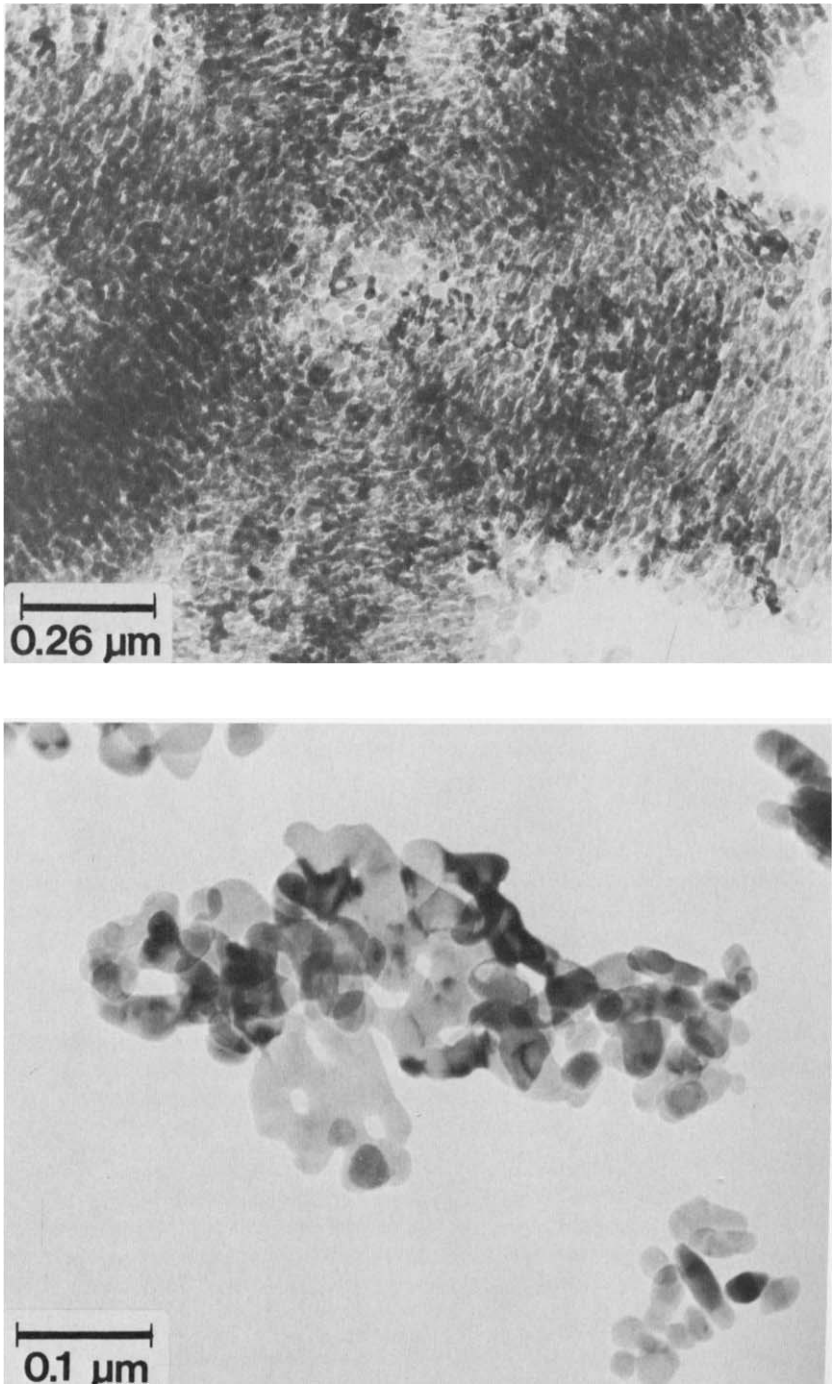

FIG. 4. Transmission electron micrographs of pure zinc oxide prepared by calcination of $Zn_5(OH)_6(CO_3)_2$ (*40*). [Reprinted with permission from *J. Catal.* **57**, 339 (1979). Copyright (1979) Academic Press, New York.]

IV. The Activity of Pure Zinc Oxide

In a similar experiment, 2.5 g of zinc oxide prepared by precipitation from zinc nitrate solution by sodium carbonate, calcination, and attempted reduction under similar conditions as previously employed, gave a catalyst of surface area of 40 m^2/g, which yielded less than 10^{-9} kg of methanol per square meter of the catalyst per hour under the standard conditions used for the testing of the copper catalyst. The zinc oxide was in its wurtzitic crystal modification as in most laboratory as well as industrial catalysts, was free of surface impurities, and had a morphology shown in Fig. 4. Details of the pore structure of this catalyst are given in reference (*38*).

The experiment outlined above demonstrates that like metallic copper, pure zinc oxide is a very poor methanol catalyst at 75 atm and 250°C. This finding contrasts with the relatively high activity of zinc oxide at pressures exceeding 200 atm and temperatures above 350°C.

Further, since the activity of zinc oxide has been found to be higher than that of other oxides such as alumina or chromia, no single-component catalyst, oxide, or metal is known at the present time that would effectively catalyze methanol synthesis at low temperatures and pressures, i.e., below 250°C and 100 atm. It is the synergic promotion in multicomponent catalysts that brings about greatly enhanced activity at low temperatures.

V. The Binary Copper–Zinc Oxide System

After the introduction of the low-pressure processes using the $Cu/ZnO/Al_2O_3$ and $Cu/ZnO/Cr_2O_3$ catalysts summarized in Tables I and II, the question arose as to what causes the high activity of these catalysts compared to that of their individual components. Herman *et al.* (*39*) investigated the relation of the activity of the single components and their binary, as well as ternary, combinations to various physical and chemical characteristics of these catalysts. They have established that the low-temperature-low pressure activity resides in the binary copper-zinc oxide system and have optimized the catalyst composition for maximum methanol yields. The catalysts were characterized in all stages of preparation and before as well as after use by X-ray diffraction, electron microscopy, Auger/ESCA spectroscopy, optical spectroscopy, BET surface-area measurements, and chemisorption measurements (*38–43*). The principal findings are summarized in the following sections.

A. Preparation of the Cu/ZnO Binary Catalysts

The catalysts were coprecipitated from Cu/Zn nitrate solutions by sodium carbonate, keeping the initial nitrate concentration constant and varying the Cu/Zn ratio from 0/100 to 100/0. In the zinc-rich compositional range hydroxy carbonates were precipitated, while in the copper-rich range the main product was copper hydroxy nitrate $Cu_2(OH)_3NO_3$. Upon calcination in air at 350°C, these precursor compounds turned into a heterophase mixture of tenorite CuO and wurtzite ZnO, and upon following reduction in 2% H_2/N_2 gas, the cupric oxide was converted to copper and the zinc oxide remained unreduced in its wurtzite modification. Although the precipitate precursors did not influence the phase composition of the calcined CuO/ZnO or the reduced Cu/ZnO catalysts, their composition determined the interdispersion and morphology of the final catalyst. A very intimate mixture of small copper and zinc oxide particles was obtained by calcination and reduction of the $(Cu, Zn)_2(OH)_2CO_3$ precursor in which copper and zinc initially occupy the same type of lattice sites and are interdispersed on atomic scale. It was this preparation that led to the formation of the most active binary catalyst (*39*).

B. Physical Characteristics of the Cu/ZnO Catalysts

A quantitative X-ray diffraction study of the Cu/ZnO catalysts (*41*) has revealed that varying amounts of copper appear in an X-ray amorphous

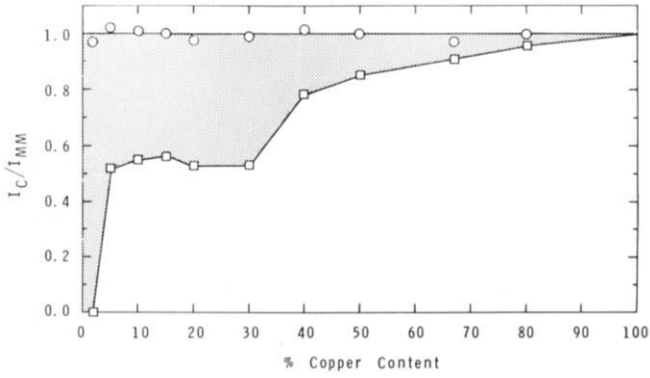

FIG. 5. Comparisons of the crystalline Cu^0 (□) and ZnO (○) components in the reduced Cu/ZnO catalysts, I_C, with those in the reduced mechanically mixed composites, I_{MM}, as determined by X-ray powder diffraction; I is the integrated intensity. Shaded area shows the fraction of amorphous copper (*41*). [Reprinted with permission from *J. Phys. Chem.* **83,** 3118 (1979). Copyright (1979) American Chemical Society.]

TABLE V
BET Argon Surface Areas of the Cu/ZnO Catalysts[a]

Catalyst composition CuO/ZnO	Surface area (m^2/g) of		Catalyst composition CuO/ZnO	Surface area (m^2/g) of	
	Reduced	Used		Reduced	Used
0/100		25.2	40/60		13.5
2/98		28.9	50/50		10.3
10/90		27.0	67/33	6.3	8.6
20/80		30.0	100/0	1.4	—
30/70		37.1			

[a] From Ref. *39*.

form, as demonstrated in Fig. 5. It is evident that the amorphous state of copper is induced by the presence of zinc oxide, since all copper metal is crystalline where zinc oxide is absent. Since the largest amounts of amorphous copper were found in the most active catalysts, it became important to further identify the location and state of this component of the catalyst. The BET surface areas are summarized in Table V. It is seen from the data in Fig. 5 and Table V that no dramatic increase of the total catalyst surface area occurs in samples with large amounts of amorphous copper, contrary to what would be expected if amorphous copper were dispersed as very small particles. The answer to the question of the location of amorphous copper was provided by a combination of structural and elemental analyses of the Cu/ZnO binaries in the scanning transmission electron microscope (STEM) (*40*). Significant amounts of copper were found in the zinc oxide phase of the catalyst; these are compared with the amount of X-ray amorphous copper in Table VI to show that most if not all the amorphous copper is located in the zinc oxide crystallites. Furthermore, this amorphous copper is not accumulated on the zinc oxide crystallite surface because the amount of oxygen and zinc determined by surface analysis in ESCA/Auger spectrometer is that expected from a uniform interdispersion of O, Zn, and Cu throughout the sample. Hence the combined STEM, ESCA/Auger, and surface-area measurements indicate that the amorphous copper is dispersed, or dissolved, in the zinc oxide phase. This result was corroborated by optical studies and further refined by chemisorption measurements discussed below.

The electronic interaction between the catalyst components is best exemplified by its color and optical spectra. For example, the very active binary catalyst Cu/ZnO = 30/70 has a pitch black color and although it is composed of crystallographically identifiable copper and zinc oxide, its optical spectrum is not a superposition of the spectrum of copper metal and zinc oxide, but rather comprises a very intense continuous absorption band in the visible part of the spectrum that contains no trace of the characteristic

TABLE VI

Extent of Cu/ZnO Solid Solution Formation in the Reduced Coprecipitated Catalyst, as Determined by X-Ray Powder Diffraction and Electron Microscopy

Nominal catalyst composition[a]	Cu (%) in solid solution		Nominal catalyst composition[a]	Cu (%) in solid solution	
	X-ray diffraction[b]	Electron microscopy[c]		X-ray diffraction[b]	Electron microscopy[c]
2/98	2.0		30/70	16.8 ± 1.5	15.1 ± 3.7
5/95	2.5		40/60	12.6 ± 1.5	5.0 ± 3.7
10/90	4.8		50/50	13.0 ± 2.0	8.7 ± 3.6
15/85	8.1		67/33	15.4 ± 3.0	11.6 ± 2.8
20/80	10.5		80/20	14.2	

[a] CuO/ZnO in wt. %.

[b] Expressed as amorphous copper/(ZnO + amorphous Cu); from Ref. *41*.

[c] From Ref. *40*.

zinc oxide absorption edge at 25,800 cm^{-1} in the near UV. There is an absorption edge in the near IR which appears at frequencies lower than those of the copper metal d-hump (*41*). This spectrum was attributed by Klier and co-workers (*39*, *41*) to the copper solution in the zinc oxide, and a physical model was put forward which is depicted in Fig. 6. The disappearance of the zinc oxide absorption edge was explained as originating from the overlap

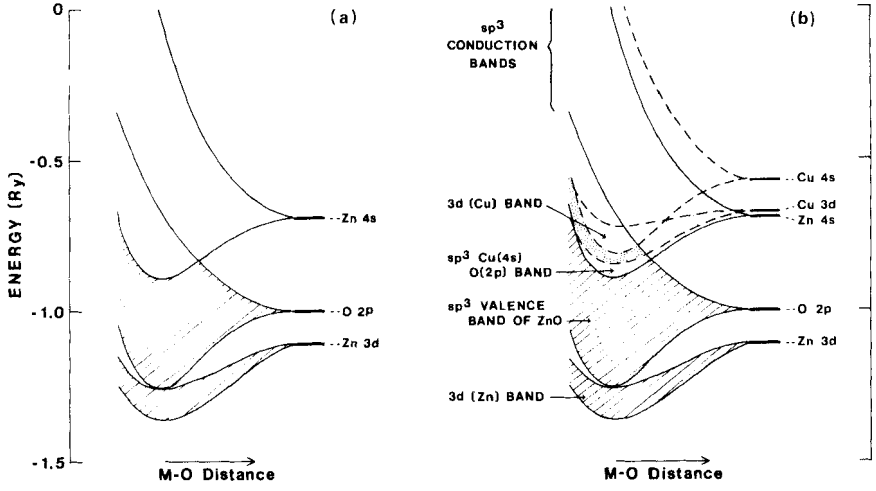

FIG. 6. A diagram showing the band spectra of (a) ZnO and (b) Cu/ZnO solid solution (*39*). [Reprinted with permission from *J. Catal.* **56**, 407 (1979). Copyright (1979) Academic Press, New York.]

of the copper solute spd band with the valence-band edge of zinc oxide, the appearance of the near-IR edge was proposed to be due to the transition between the copper dsp band and the conduction band of the zinc oxide, and the high intensity of the transition was attributed to the high degree of allow that also is characteristic of the UV band-to-band transition in the pure zinc oxide.

The copper solution in the zinc oxide characterized by the outlined analytical and physical methods was found to exist only after mild reduction of the calcined catalyst. Before reduction, the solubility of CuO in ZnO is limited to 4–6% (*44*, *45*) and after more severe reduction, the optical spectra begin to resemble a superposition of those of pure copper metal and zinc oxide. Hence the black solute phase is metastable and does not appear to be the final product of reduction. For this reason, the dispersed copper species were assigned the valence state +1; Bulko *et al.* (*41*) visualized these copper species not as isolated Cu^+ ions but rather as electron-deficient copper atoms with strong electronic overlap with the host zinc oxide lattice, particularly with neighboring oxygens whose orbitals dominate in the valence band of zinc oxide.

C. Particle Size and Morphology

Using the preparation method described above, the particle sizes of the crystalline components of the Cu/ZnO catalyst were strongly determined by the precursor composition and structure. Figure 7 shows that small particles of CuO, copper, and zinc oxide formed by calcination and reduction of hydroxy carbonate precursors at concentrations Cu/ZnO = 0/100 to 30/70, while large particles of all components result from calcination and reduction of precursors that contain copper hydroxy nitrate at compositions Cu/ZnO = 40/60 to 100/0. The rather sudden change of particle size between compositions Cu/ZnO = 30/70 and 40/60 is accompanied by interesting changes of morphology which are demonstrated in the electron micrographs of the Cu/ZnO = 30/70 (Fig. 8) and 67/33 (Fig. 9) catalysts (*40*). In the zinc-rich region, zinc oxide forms intertwined lacework with the hexagonal crystal axis parallel to its longer dimension, while in the copper-rich composites, zinc oxide crystallizes as well-shaped hexagonal platelet crystals with their major crystal axis perpendicular to the platelet plane. The hexagonal platelet morphology of zinc oxide is believed to originate during the thermal decomposition of hydroxy carbonates and hydroxy nitrates of zinc and copper. Since the hydroxy carbonates that are rich in zinc decompose at slightly lower temperatures than hydroxy nitrate of copper, the zinc oxide crystals can epitaxially nucleate on the pseudohexagonal (001) plane of

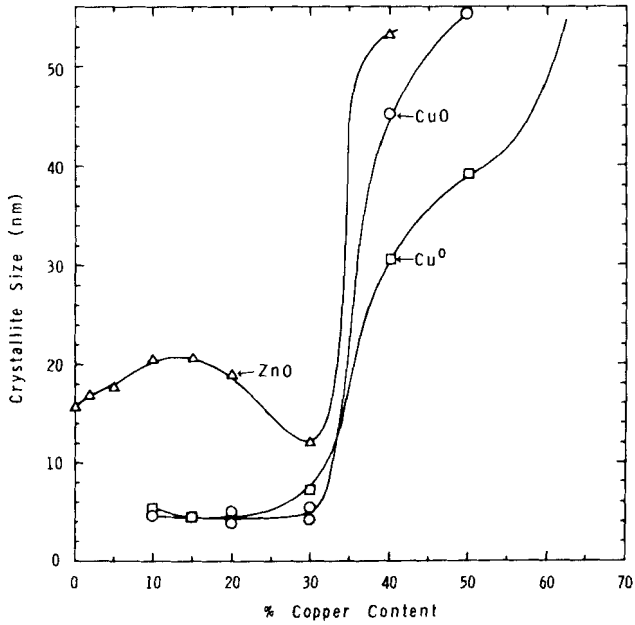

FIG. 7. The average particle sizes of copper (□), its CuO precursor (○), and zinc oxide (△) determined from X-ray diffraction line broadening (*41*). [Reprinted with permission from *J. Phys. Chem.* **83,** 3118 (1979). Copyright (1979) American Chemical Society.]

$Cu_2(OH)_3NO_3$, giving rise to the hexagonal ZnO crystals. In subsequent stages of calcination the copper hydroxy nitrate decomposes to form separate particles of CuO. Further interesting details are also apparent from the electron microscope investigations of Mehta *et al.* (*40*). Figure 8 shows that copper particles are in intimate contact with zinc oxide in the 30/70 catalyst. Moreover, these particles are in epitaxial registry with the zinc oxide crystallites, as demonstrated by the selected area diffraction pattern in Fig. 10. The spot pattern indicates that the whole zinc oxide lacework is single-crystal oriented with its hexagonal axis parallel to the edge of the particle assembly marked in Fig. 8. Furthermore, the copper crystallites are in definite crystallographic orientation with respect to the zinc oxide and to each other. The Cu/ZnO = 30/70 catalyst is thus composed of zinc oxide exposing its $(10\bar{1}0)$ prism planes with the copper particles being spherical caps facing the underlying zinc oxide with their (211) planes. In addition to these structural features, a large amount of copper (15% in the 30/70 catalyst) was found to be located in the zinc oxide phase by 6-nm spot analyses in STEM (*40*). This amount coincides, within analytical error, with the amount of amorphous copper determined by X-ray diffraction as shown in Table VI.

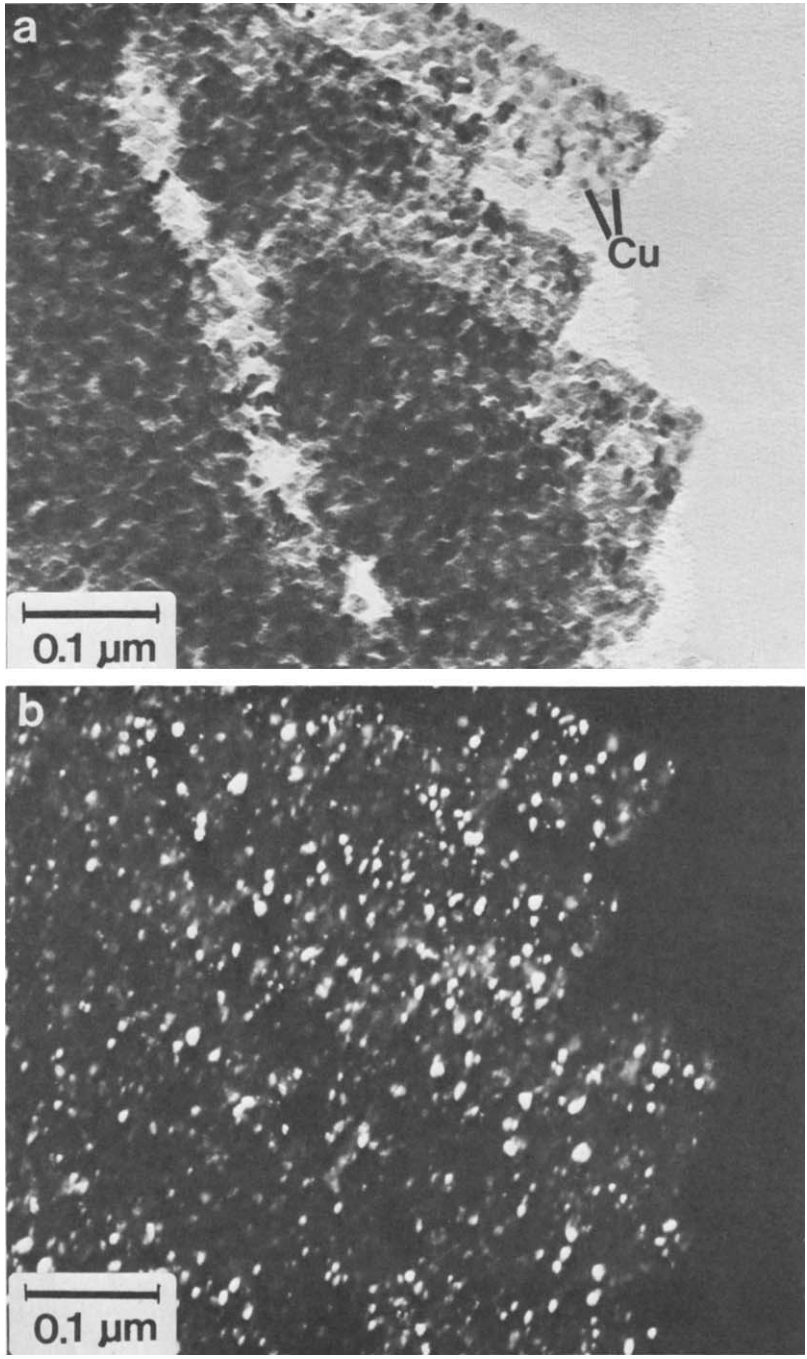

FIG. 8. (a) Transmission electron micrograph of a Cu/ZnO = 30/70 binary catalyst (*40*); 60 Å copper spheres are placed on crystalline zinc oxide network. (b) Dark field image of the copper crystallites in the area shown in the bright field image (a) obtained using the [$\bar{1}$11] reflection of copper. [Adapted with permission from *J. Catal.* **57**, 339 (1979). Copyright (1979) Academic Press, New York.]

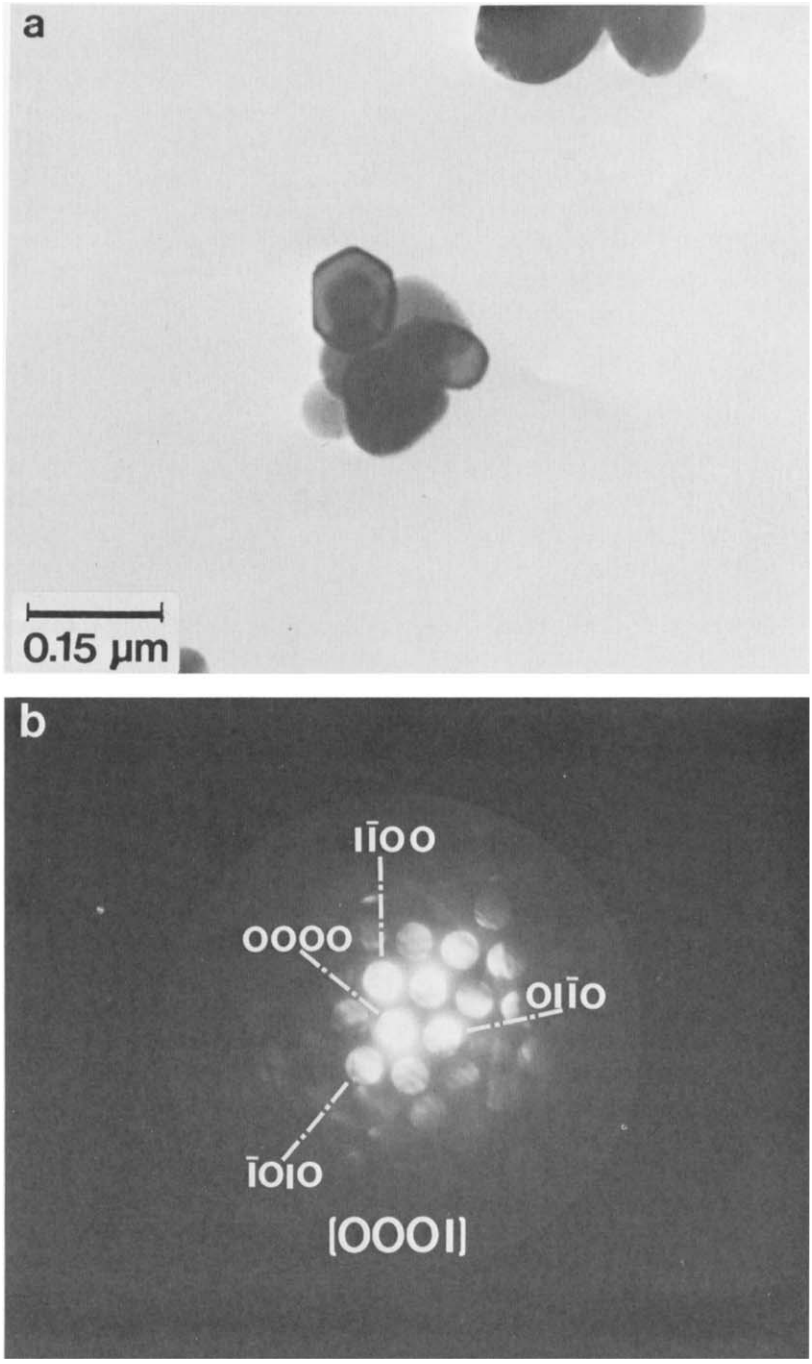

FIG. 9. (a) Transmission electron micrograph of Cu/ZnO = 67/33 catalyst. The hexagonal platelet particles are zinc oxide exposing its basal plane (0001) and the dark irregularly shaped particles are metallic copper (*40*). (b) Convergent beam diffraction pattern in STEM from the hexagonal ZnO particle shown in (a) above demonstrating that the sixfold (0001) crystal axis is perpendicular to the plane of the platelet. [Adapted with permission from *J. Catal.* **57,** 339 (1979). Copyright (1979) Academic Press, New York.]

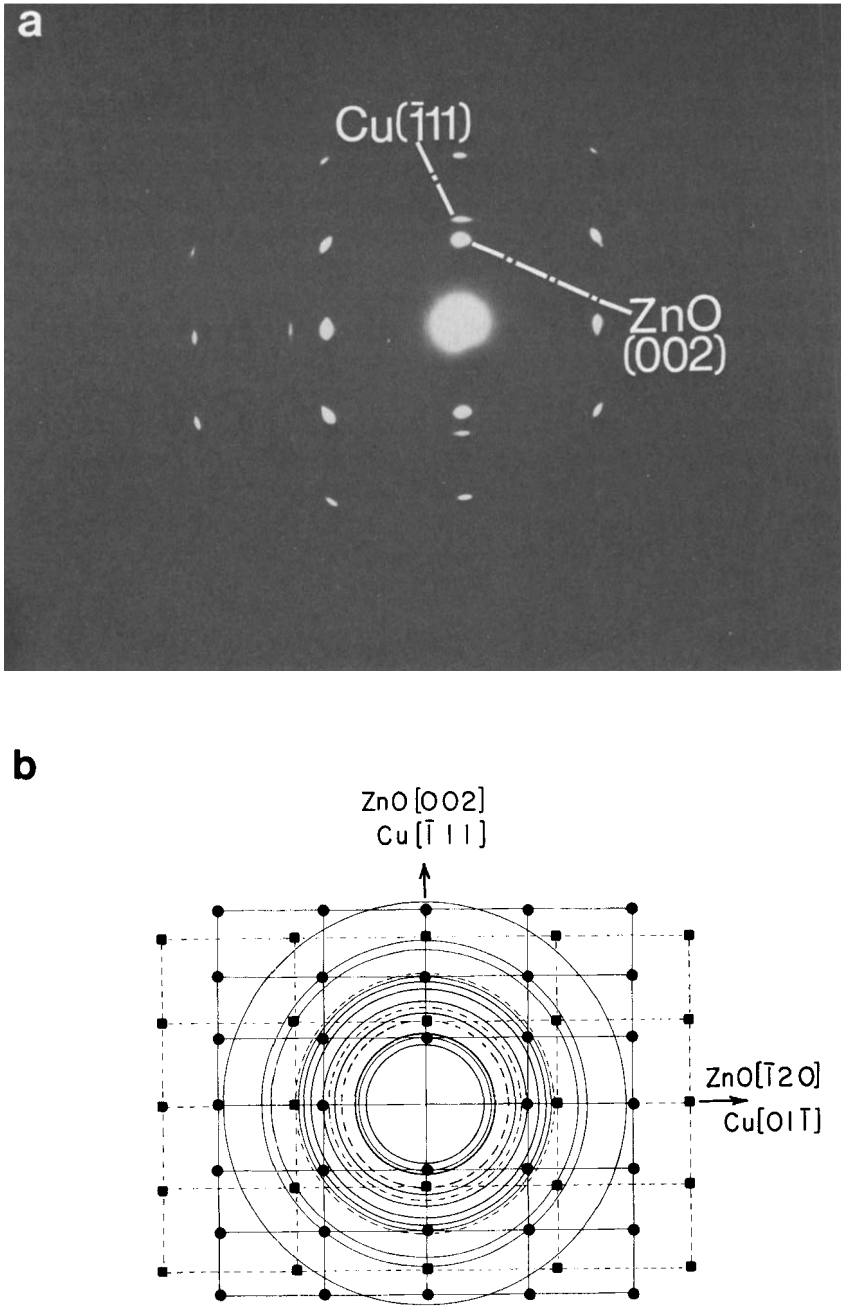

FIG. 10. (a) Selected area diffraction pattern of the reduced Cu/ZnO = 30/70 catalyst from an area shown in the upper part of Fig. 8; (b) schematic diffraction pattern showing the spots from ZnO (●) and Cu (■). The circles with the solid lines and the circles with dashed lines are the more intense diffraction rings from ZnO and Cu, respectively (*40*). [Adapted with permission from *J. Catal.* **57**, 339 (1979). Copyright (1979) Academic Press, New York.]

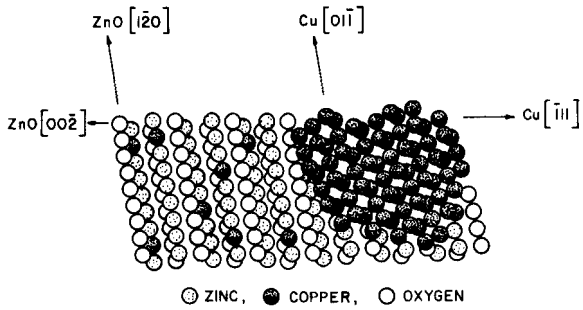

FIG. 11. A view of copper and zinc oxide crystallites with dispersed copper ions in the binary Cu/ZnO catalyst = 30/70 derived from diffraction and characteristic X-ray emission analysis in TEM and STEM.

The structural and analytical findings concerning the Cu/ZnO = 30/70 catalyst are summarily represented in Fig. 11. It is seen that this catalyst has several parts to be considered as potential seats of catalytic activity: the copper crystallite surface, the zinc crystallite surface, the copper solute in zinc oxide, and finally the interface between the copper and zinc oxide particles. To resolve which constituent of this catalyst is mainly responsible for its activity, it is helpful to examine the structural and compositional features of the second morphologic range at compositions Cu/ZnO = 40/60 and at higher copper concentrations. The ZnO particles are hexagonal platelets exposing their (0001) basal planes as major faces, and copper is in the form of large irregular blunted particles. The copper and zinc oxide particles are well separated and there appears little contact between the two phases (see Fig. 9). However, the zinc oxide particles again contain significant amounts of dispersed copper (*40*). Since Cu/ZnO = 67/33 also is an active catalyst, the copper solute appears to be a species of prime importance, and the contact between copper and zinc oxide crystals seem to play at most a secondary role in the formation of the active catalyst. This issue will be discussed further in conjunction with the chemisorption and activity measurements.

D. Surface Analysis by XPS–Auger Spectroscopy

Elemental surface composition of the same Cu/ZnO catalysts as those investigated by other methods and tested for methanol synthesis was determined by X-ray photoelectron (XPS) and Auger spectroscopy and reported by Herman *et al.* (*39*). The catalysts show surface concentrations of Cu, Zn, and O that roughly correspond to their nominal elemental compositions. Given the semiquantitative nature of electron spectroscopic analysis and the

effect of particle shape on the effective analytical cross sections for the individual elements, subtle changes of concentration ratios cannot be determined reliably. However, it is evident that there is no dramatic redistribution of elements between the bulk and the surface of the catalyst particles such as might be expected to occur if copper were to form overlayers on the zinc oxide surface or if zinc oxide were to form a "coating" on the copper particles.

In principle, Auger/XPS analysis can be used for the determination of valence states of the catalyst components in various stages of reduction and use in the synthesis reaction. These refined analyses are in progress in the author's laboratory and their results will be reported in future communications. At this time the analysis indicates that no cupric ions or zinc metal atoms are present at any stage of reduction or synthesis at temperatures including and below 250°C.

The possible surface contaminations were carefully followed by Auger–XPS analysis. Similarly, as with the copper catalyst described earlier (Section III) the Cu/ZnO binaries were free from alkali metals, iron, chlorine, and sulfur, and contained only small amounts of carbon after the use in catalytic reactor (*39*). The latter result indicates that reactants, intermediates, and the product are adsorbed with moderate strength, a feature that is desirable for all efficient catalysts.

E. Surface Areas of the Individual Catalyst Components

Many researchers have argued that the activity of the low-temperature methanol catalysts is associated solely with the copper surface (*27*, *46*, *47*). Although the experiment using unsupported copper (Section III) indicates otherwise, it is still desirable to determine the copper surface area in the supported catalysts. Among the several methods offered in the literature, low-temperature oxygen chemisorption has been most widely used. Most investigators agree that oxygen irreversibly chemisorbed on copper at temperatures lower than 140 K occupies an area of around 0.16 nm^2 per oxygen atom, based on 0.14 nm^2 for argon area (*48*), which corresponds approximately to a formula Cu_2O. The method has been used to measure surface areas of pure copper (*48*, *49*), and of copper in the $Cu/ZnO/Al_2O_3$ catalysts (*27*, *50*). Parris and Klier (*43*) used oxygen chemisorption to determine copper areas in the binary Cu/ZnO catalysts. Oxygen chemisorbed irreversibly at 78 K was found to cover an area of 15.2 $Å^2$ per oxygen atom on pure copper, and this value was also assumed to hold for copper surface in the Cu/ZnO composites. No irreversible oxygen was found on pure zinc oxide. The zinc oxide area was then calculated as the difference between the total

TABLE VII
Area of Copper Metal and Zinc Oxide in the Binary Cu/ZnO Catalysis[a]

Catalyst composition Cu/ZnO	Surface area (m^2/g catalyst)			Catalyst composition Cu/ZnO	Surface area (m^2/g catalyst)		
	Cu	ZnO	Total		Cu	ZnO	Total
0/100	—	24.1	24.1	40/60	6.5	8.5	15.0
10/90	4.9	30.1	35.0	50/50	5.7	5.4	11.1
20/80	8.9	27.6	36.5	67/33	3.9	3.5	7.4
30/70	16.0	23.3	39.3	100/0	0.62	—	0.62

[a] Parris and Klier (*43*).

BET area (Table V) and the copper area from oxygen chemisorption. Table VII summarizes the copper and zinc oxide areas so determined for the whole compositional range. The oxygen chemisorption method suffers from the uncertainty that some oxygen may be adsorbed on the copper solute and on defects in the zinc oxide surface that are formed only in the presence of copper. There is indirect evidence from a comparative study of carbon monoxide and oxygen chemisorption, however, that this is not the case and that oxygen titrates only the copper metal surface.

F. Chemisorption of Carbon Monoxide and Hydrogen

Quantitative and qualitative changes in chemisorption of the reactants in methanol synthesis occur as a consequence of the chemical and physical interactions of the components of the copper–zinc oxide binary catalysts. Parris and Klier (*43*) have found that irreversible chemisorption of carbon monoxide is induced in the copper–zinc oxide catalysts, while pure copper chemisorbs CO only reversibly and pure zinc oxide does not chemisorb this gas at all at ambient temperature. The CO chemisorption isotherms are shown in Fig. 12, and the variations of total CO adsorption at saturation and its irreversible portion with the Cu/ZnO ratio are displayed in Fig. 13. The irreversible portion was defined as one which could not be removed by 10 min pumping at 10^{-6} Torr at room temperature. The weakly adsorbed CO, given by the difference between the total and irreversible CO adsorption, correlated linearly with the amount of irreversibly chemisorbed oxygen, as demonstrated in Fig. 14. The most straightforward interpretation of this correlation is that both irreversible oxygen and reversible CO adsorb on the copper metal surface. The stoichiometry is approximately CO:O = 1:2, a ratio obtained for pure copper, over the whole compositional range of the

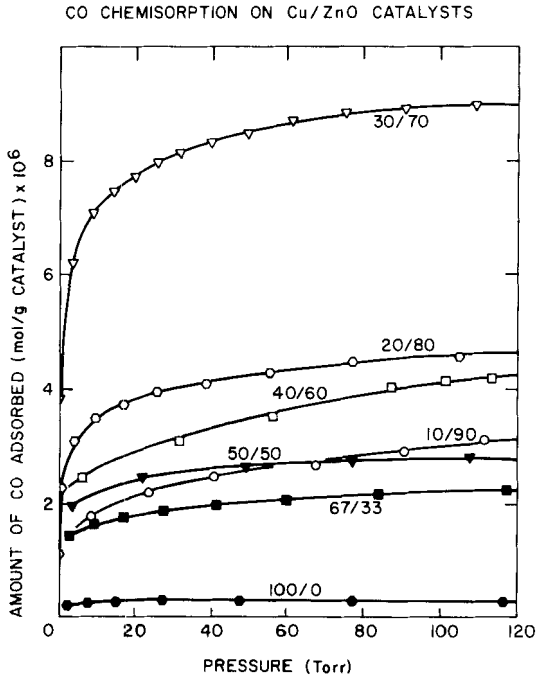

FIG. 12. Carbon monoxide chemisorption isotherms at 25°C on the binary Cu/ZnO catalysts. The labels at the individual isotherms denote the molar composition Cu/ZnO (*43*).

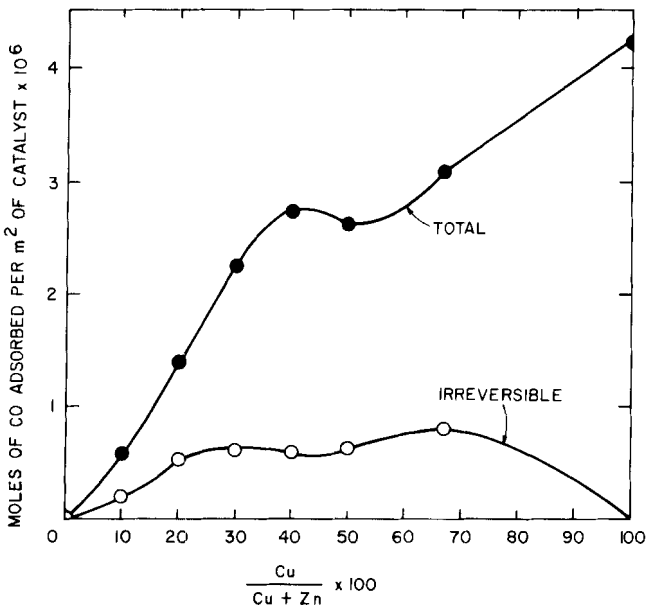

FIG. 13. The dependence of the carbon monoxide saturation adsorption (total) and irreversible adsorption (irreversible) on the Cu/ZnO ratio in the binary copper–zinc oxide catalysts (*43*).

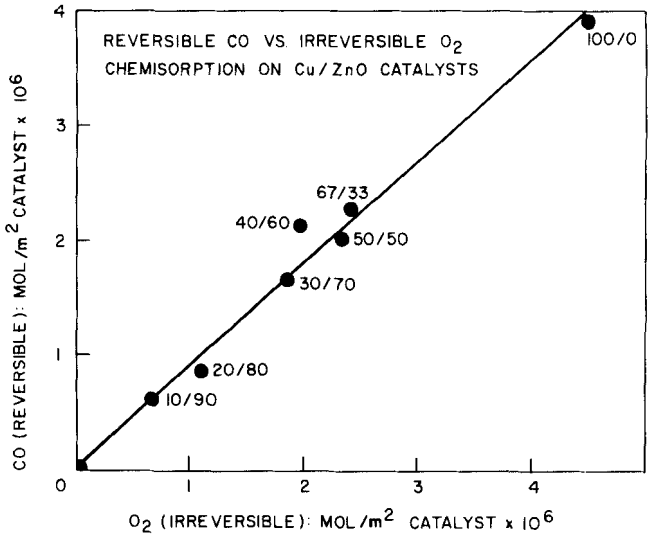

FIG. 14. The relation between the amounts of weakly chemisorbed carbon monoxide and irreversibly chemisorbed oxygen, indicating that these two adsorbates are a measure of copper metal surface area (*43*).

Cu/ZnO catalysts. Furthermore, sites other than copper metal must be available for the irreversible CO, and it was suggested by Parris and Klier that these are the copper solute sites in the zinc oxide surface. The plot of the surface coverage by irreversible CO against the concentration of copper solute shown in Fig. 15 has a linear portion for each morphology of zinc oxide. Therefore, if the irreversibly bound CO molecules titrate the surface copper solute sites, the basal (0001) ZnO planes tend to accumulate more of the solute copper atoms than the prism ($10\bar{1}0$) planes. Since the basal plane is formally electrostatically charged while the prism plane is not, the accumulation of copper is consistent with the notion that the solute copper species are also charged and tend to neutralize the excess charges of the basal planes of zinc oxide. These copper ions are then considered to be the active centers for the irreversibly chemisorbed carbon monoxide. The catalysts containing the hexagonal zinc oxide platelets are more complex than the catalysts with prism morphology for two reasons: first, in addition to the basal planes, the platelets also expose the prism faces, and their chemisorption activity will be a superposition of the two; and second, the basal planes may be composed of oxygen- and zinc-rich patches as has often been reported for hexagonal crystals (*51*, *52*). Despite this complexity, however, catalysts with hexagonal-platelet zinc oxide morphology may be of practical value in applications where low-surface-area catalysts are desired, such as in liquid-

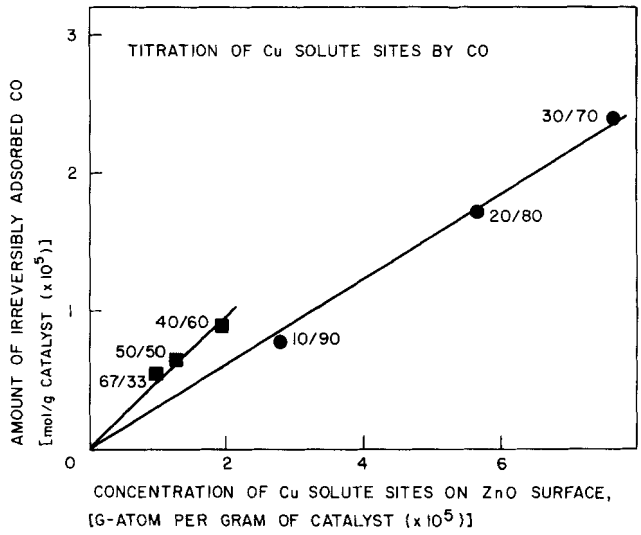

FIG. 15. The dependence of the amount of irreversibly chemisorbed carbon monoxide on the concentration of amorphous copper found by X-ray diffraction (Fig. 5) and by STEM (Table VI). The $(10\bar{1}0)$ prism planes of zinc oxide are exposed in the Cu/ZnO = 10/90, 20/80, and 30/70 catalysts and the (0001) basal planes of ZnO are exposed in the Cu/ZnO = 40/60, 50/50, and 67/33 catalysts. The different slopes for the two morphologies indicate slightly different concentrations of copper atoms on the prism and basal surfaces (*43*).

phase methanol synthesis (*53*). Of these composites, the Cu/ZnO = 67/33 of surface area of only 7–9 m^2/g proved quite an effective irreversible sorbent for CO and, as is shown below, a catalyst of the highest specific activity.

G. Activity Patterns

All the binary Cu/ZnO catalysts were found highly selective toward methanol without DME, methane, or higher alcohols and hydrocarbons detected in the product by sensitive gas chromatographic methods (*39*). Several of the composites were also found to be very active when subjected to a standard test with synthesis gas $CO/CO_2/H_2$ = 24/6/70 at gas hourly space velocity of 5000 hr^{-1}, pressure 75 atm, and temperature 250°C. The activities, expressed as carbon conversions and yields, are summarized in Table VIII. The end members of the series, pure copper and pure zinc oxide, were inactive under these testing conditions, and maximum activity was obtained for the composition Cu/ZnO = 30/70. The yields per unit weight, per unit area of the catalyst or the individual components, turnover rates per site titratable by irreversible oxygen and by irreversible carbon monoxide, are graphically

TABLE VIII
The Catalytic Testing Results for the Cu/ZnO Systems[a]

Catalyst composition[b] $CuO/ZnO/M_2O_3$	Carbon conversion	Yield		
		kg liter^{-1} hr^{-1}	kg kg^{-1} hr^{-1}	kg m^{-2} hr^{-1} ($\times 10^5$)
0/100/0	0	0	0	0
2/98/0	0.7	0.02	0.03	0.10
10/90/0	1.0	0.02	0.02	0.70
20/80/0	10.2	0.22	0.24	0.80
30/70/0	51.1	1.10	1.35	3.63
40/60/0	9.6	0.21	0.18	1.33
50/50/0	11.3	0.25	0.20	1.94
67/33/0	21.8	0.48	0.41	4.76
100/0/0	0	0	0	0
60/30/10[c]	40.0	0.95	1.52	5.82
60/30/10[d]	17.0	0.45	0.58	1.73
60/30/10[e]	47.0	1.17	1.01	6.47

[a] Obtained at 250°C, 75 atm, and GHSV = 5000 hr^{-1} with a synthesis gas of $H_2/CO/CO_2$ = 70/24/6 vol%. From Ref. *39*.
[b] Weight percent as the oxides.
[c] M = Al, prepared from the acetates.
[d] M = Al, prepared from the nitrates, tested at 100 atm.
[e] M = Cr, tested at 100 atm.

represented in Fig. 16. Aside from showing that the active catalyst indeed requires the simultaneous presence of zinc oxide and copper, these graphs indicate that no single component surface is responsible for the activity. For example, should only copper metal or only zinc oxide be the active component, the activities per unit area of copper or zinc oxide would be independent of the composition. The reasons for the lack of constancy of the specific activities and turnover frequencies defined and presented in various ways in Fig. 16 must be sought, therefore, in the interactions of the catalyst components that give rise to the active catalyst.

Several observations have already indicated that the amorphous copper solute induces irreversible chemisorption of carbon monoxide, and it therefore behooves us to correlate the methanol yields with the surface concentration of irreversibly chemisorbed CO. The best understanding of the synthesis pattern is provided with the help of the representation in Fig. 17. The turnover rate, defined as the number of CO molecules converted to methanol in 1 sec on one site titratable by irreversibly bound carbon monoxide, depends smoothly on the concentration of these sites for each zinc

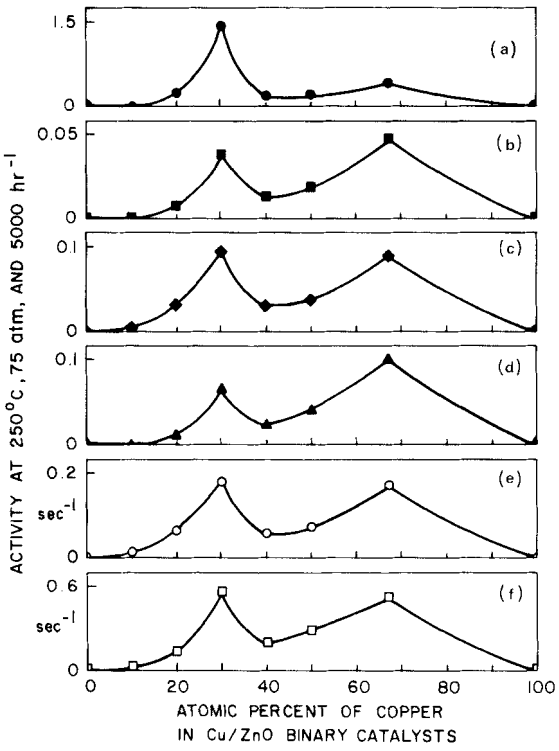

FIG. 16. Catalytic activity expressed as yield of methanol per unit weight, per unit surface area of the Cu/ZnO catalyst, per unit surface areas of the components Cu and ZnO, and as turnover numbers over copper metal sites titratable by irreversible adsorption of oxygen and over Cu/ZnO solute titratable by irreversible adsorption of carbon monoxide: (a) g MeOH/g catalyst hr^{-1}; (b) g MeOH/m^2 catalyst hr^{-1}; (c) g MeOH/m^2 Cu hr^{-1}; (d) g MeOH/m^2 ZnO hr^{-1}; (e) turnover rate per oxygen site; (f) turnover rate per carbon monoxide site.

oxide morphology, i.e., for the prism morphology in the compositional range Cu/ZnO = 10/90 to 30/70, and for the hexagonal platelet morphology for Cu/ZnO = 40/60 to 67/33. At the same time, the turnover rate varies as the second to third power of the surface site concentration, indicating that three to four sites are involved in the conversion of each CO molecule. This is possible if one site is utilized for activation of carbon monoxide and several other sites for activation of hydrogen. Since the sites titrated by irreversibly adsorbed CO are fairly diluted ($\leq 6 \times 10^{17}/m^2$ ZnO for the prism morphology and $\leq 1 \times 10^{18}/m^2$ ZnO for the basal morphology; see Fig. 17), the activated reaction components must have a significant lateral mobility to reach the site of reactive encounter.

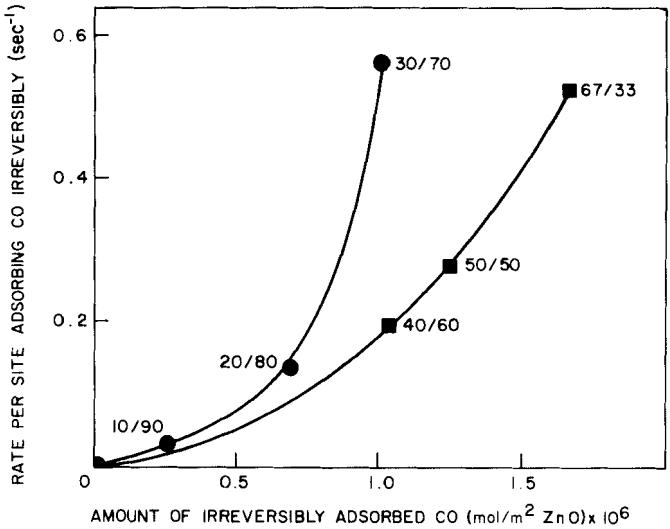

FIG. 17. The dependence of turnover rates of methanol synthesis (at 250°C, 75 atm) over sites binding carbon monoxide irreversibly upon the concentration of these sites on ZnO surface (*43*).

To summarize the qualitative findings, the methanol synthesis activity in the binary Cu/ZnO catalysts appears to be linked to sites that also irreversibly chemisorb CO and not to sites that adsorb CO reversibly. Since irreversible adsorption of CO follows linearly the concentration of amorphous copper in zinc oxide, these sites are likely to be that part of the copper solute that is present on the zinc oxide surface. No correlation of the catalyst activity and the copper metal surface area, titrated by reversible form of CO or by oxygen, could be found in the binary Cu/ZnO catalysts (*43*). In contrast with this result, it has been claimed that the synthesis activity is proportional to copper metal area in copper–chromia (*47*), copper–zinc aluminate (*27*), and copper–zinc oxide–alumina (*46*) catalysts. In these latter communications (*27*, *46*, *47*), the amount of amorphous copper has not been determined, and obviously there is much room for further research to confirm one or another set of results and interpretations. However, in view of the lack of activity of pure copper metal quoted earlier, it is unlikely that the synthesis activity is simply proportional to the copper metal surface area in any of the low-temperature methanol-synthesis catalysts.

H. Reaction Kinetics in the Presence of Carbon Dioxide

It has been known for some time that a small amount of carbon dioxide in the CO/H_2 synthesis gas acts as a promoter or prevents catalyst deactivation

(*27*, *39*). This effect was attributed to the ability of CO_2 to keep the catalyst in its intermediate oxidation state such as Cu(I) (*39*), or to prevent reduction of zinc oxide with concomitant formation of brass (*27*), or to the reversal of the Boudouart reaction

$$2CO \rightleftharpoons CO_2 + C \tag{4}$$

that would cause carbon fouling of the catalyst. However, by Auger spectroscopy Simmons (*54*) found very little carbon and no carbidic species on the Cu/ZnO catalyst exposed to the CO_2-free CO/H_2 synthesis gas and Chatikavanij (*55*) did not detect any traces of methane, which would be expected to form by hydrogenation of surface carbon, when running the synthesis in $CO/H_2 = 30/70$ synthesis gas. Hence, the Boudouart reaction is an unlikely cause of catalyst deactivation in the CO_2-free synthesis gas. That the CO_2 enhancement of the synthesis rate is a true chemical promotion effect of CO_2 and not a kinetic effect that would be produced by an addition of any inert has been established by replacing CO_2 by Ar, whereupon the CO conversion rate decreased by a factor 4.5 (*56*). In pursuing the effects of CO_2 further, it was found that there is an optimum in the CO_2/CO ratio at which the synthesis runs at maximum rate (*56*, *27*). At high concentrations, CO_2 has a gradually retarding effect on the synthesis (*27*, *56*).

The influence of the CO_2/CO ratio on the synthesis has been embedded in kinetic equations only recently. The early kinetic equations for the high-pressure ZnO/Cr_2O_3 catalyst did not contain a CO_2-dependent term at all, perhaps because the effects of CO_2 were not significant when zinc chromite catalysts were used; Natta *et al.* (*57*) proposed the rate equation for the ZnO/Cr_2O_3 catalyst at temperatures 300–360°C as follows:

$$r = \frac{\gamma_{CO} p_{CO} \gamma_{H_2}^2 p_{H_2}^2 - \gamma_{CH_3OH} p_{CH_3OH} / K_{eq}}{(A + B\gamma_{CO} p_{CO} + C\gamma_{H_2} p_{H_2} + D\gamma_{CH_3OH} p_{CH_3OH})^3} \tag{5}$$

where r is the rate of methanol synthesis; γ_i is the fugacity coefficient of species i; p_i is the partial pressure of species i; K_{eq} is the equilibrium constant of carbon monoxide hydrogenation to methanol; and A, B, C, and D are empirical constants. Equation (5) was derived under the assumption that the rate-controlling step of the synthesis is the trimolecular reaction of carbon monoxide with two hydrogen molecules in the adsorbed phase. Following Natta's publication of his data and kinetic treatment, a number of empirical as well as model-derived rate equations for methanol synthesis have been proposed, some of which have demonstrated that Natta's original data could be fitted with several kinetic models. These developments were summarized by Denny and Whan (*26*) up to 1977.

When the synthesis was carried out with carbon dioxide-rich synthesis gas, however, the comparison of measured rates with those calculated using kinetic equation (5) or its modifications (*58*) showed a substantial disparity (*59*), and it was realized that carbon dioxide-dependent terms had to be incorporated in order for the kinetic equations to be useful for process design. This was accomplished by Bakemeier *et al.* (*60*) who obtained the following rate equation, once again for the ZnO/Cr_2O_3 catalyst:

$$r = Ae^{-E/RT} \frac{p_{CO}^{n} p_{H_2}^{m} [1 - p_{CH_3OH}/(p_{CO} p_{H_2}^{2} K_{eq})]}{1 + De^{F/RT} p_{CO_2}/p_{H_2}} \tag{6}$$

In equation (6) the quantities A, E, n, m, D, and F are semiempirical parameters. It can be seen that this rate equation predicts that the methanol yield would decrease as the CO_2 partial pressure is increased and would drop to zero for synthesis gas that contains carbon dioxide only. Hence Eq. (6) describes a process in which carbon dioxide is a retardant but not at all a reactant or a promoter.

In 1973, Leonov *et al.* (*61*) introduced a kinetic rate equation for the low-pressure copper–zinc oxide–alumina catalyst for temperatures between 220 and 260°C. The rate equation was proposed to be

$$r = k \left[\frac{p_{CH}^{0.5} p_{H_2}}{p_{CH_3OH}^{0.66}} - \frac{p_{CH_3OH}^{0.34}}{p_{CO}^{0.5} p_{H_2} K_{eq}} \right] \tag{7}$$

where k is the rate constant for the forward reaction and K_{eq} is the equilibrium constant. Similar to the early kinetic studies with the high-pressure ZnO/Cr_2O_3 catalysts, there are no CO_2-dependent terms in Eq. (7) for the low-pressure synthesis.

Denny and Whan (*26*) also reviewed various contrasting reports on the effects of CO_2 on the synthesis and emphasized that any complete kinetic expression should include a term involving the partial pressure of CO_2. A rate equation that does contain an empirical CO_2-dependent term for the copper–zinc oxide–alumina catalysts has been presented in 1980 by Andrew (*27*) in the form

$$r = k p_{CO}^{0.2-0.6} p_{H_2}^{0.7} \Phi_{CO_2} \tag{8}$$

Although the function Φ_{CO_2} was not explicitly determined, it was reported that the rate of methanol synthesis reached a maximum at the CO_2:CO partial pressure ratio around 0.01–0.03 and decreased as the CO_2 pressure was further increased. It was also indicated that the methanol synthesis rate would decline at very small concentrations of CO_2. Behavior like this was

also reported to be the property of the binary Cu/ZnO catalysts (*39*), and hence it seems established that an optimum concentration of CO_2, or a ratio of CO_2 and CO concentrations, exists at which the low-pressure synthesis runs at its maximum rate. A feature common to all kinetic equations summarized above is that the forward rate is proportional to a power of the product $p_{CO} \cdot p_{H_2}^2$. When the reaction is carried out a low conversions, the reverse reaction is negligible, and the dependence of the synthesis rate on the product $p_{CO} \cdot p_{H_2}^2$, such as illustrated in Fig. 18 for the $Cu/ZnO/Cr_2O_3$ catalyst, is strong evidence that several sites are involved in one molecular synthesis step.

Klier *et al.* (*56*) presented a kinetic model based on previous observations of the physical and chemical characteristics of the binary Cu/ZnO catalysts and put forward equations that quantitatively account for the CO_2/CO dependence of the synthesis rates. Their model was required to accommodate the following observations:

1. The increase of methanol conversion rates from the CO/H_2 synthesis gas upon additions of 1–2% CO_2 can also be obtained by additions of hundredths of percent of oxygen.
2. A catalyst that has been reduced by hydrogen at 250°C can be further reduced by CO with the appearance of CO_2. When this CO-reduced catalyst is exposed to CO_2, also at 250°C, it is reoxidized and CO_2 is converted to CO. The CO/CO_2 equilibria are established in the time frame of hours (*42*).
3. The activity of the catalyst increases as a high power of the concentration of the amorphous copper, as is seen from Fig. 17, and does not depend monotonously on the surface area of crystalline copper particles.

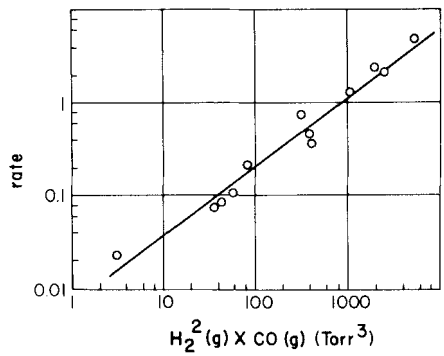

FIG. 18. Methanol synthesis rate as a function of the product of concentrations $[H_2(g)]^2 \times [CO(g)]$ over a $Cu/ZnO/Cr_2O_3$ catalyst at 250°C (*114*). [Reprinted with permission from *Bull. Chem. Soc. Jpn.* **38**, 1727 (1965). Copyright (1965) Chemical Society, Japan.]

4. Carbon dioxide is adsorbed quite strongly. The reactant adsorption strengths are estimated to decrease in the order $CO_2 > CO > H_2$.

Based on these observations, Klier *et al.* (*56*) formulated the model for the synthesis as follows:

(*i*) The catalyst can exist in a reduced state A_{red} and in an oxidized state A_{ox}. The oxidized state is active and the reduced state is inactive (cf. observation 1 above). The proportion of A_{ox} and A_{red} is controlled by the ratio of CO_2 and CO in the synthesis gas (cf. observation 2).

(*ii*) Several active centers A_{ox} are involved in each reaction step. These centers may be identified with copper solute species in zinc oxide (cf. observation 3).

(*iii*) All three components of the synthesis gas CO, H_2, and CO_2 react in the adsorbed layer; CO_2 competes for active sites with at least one of the reactants CO and H_2. The adsorption strengths are in the order $CO_2 > CO > H_2$ (cf. observation 4).

The redox reaction that controls the concentration of the active form A_{ox} can be written as

$$A_{ox} + CO(g) \rightleftharpoons A_{red} + CO_2(g) \tag{9}$$

which together with the requirement that the reduced and oxidized forms of the catalyst sum up to a constant $A_0 = A_{red} + A_{ox}$, yields for the concentration of active centers

$$A_{ox} = A_0 \frac{K'(p_{CO_2}/p_{CO})}{1 + K'(p_{CO_2}/p_{CO})} \tag{10}$$

Klier *et al.* investigated several cases of kinetics in which methanol is formed by a surface reaction between CO and hydrogen adsorbed on the A_{ox} sites competitively or noncompetitively with CO on the A_{ox} sites and hydrogen elsewhere on the surface; in each case CO_2 effects *sub* (*i*) and (*iii*) above were taken into account. In addition, it was found empirically that a small amount of CO_2 is hydrogenated to methanol at a rate that linearly depended on partial pressure of CO_2. All kinetic equations that successfully described the CO_2 effects had the general form

$$r = \text{const } A_{ox}^m \frac{p_{CO}p_{H_2}^2 - p_{MeOH}/K_{eq}}{(F + K_{CO_2}p_{CO_2})^n} + k'[p_{CO_2} - (K'_{eq})^{-1}(p_{MeOH}p_{H_2O}/p_{H_2}^3)] \tag{11}$$

where F is a linear function of pressures of H_2, CO, H_2O, and CH_3OH; the exponent m is close to 3; the exponent n ranges from 1 to 3; and A_{ox} is determined by the ratio p_{CO_2}/p_{CO} as shown in Eq. (10). The term K_{eq} is an equilibrium constant, defined by partial pressures, for the reaction (1) and K'_{eq} for the reaction (2). These constants are related to fugacity ratios K_γ and K'_γ and to the true equilibrium constants K_p and K'_p as $K_{eq} = K_p/K_\gamma$; $K'_{eq} = K'_p/K'_\gamma$, and their pressure–temperature dependences are given by (*5*, *56*)

$$\begin{aligned} K_p &= 3.27 \times 10^{-13} \exp(11{,}678/T), & K'_p &= 3.826 \times 10^{-11} \exp(6851/T) \\ K_\gamma &= 1 - A_1 P, & K'_\gamma &= (1 - A_1 P)(1 - A_2 P) \\ A_1 &= 1.95 \times 10^{-4} \exp(1703/T), & A_2 &= 4.24 \times 10^{-4} \exp(1107/T) \end{aligned} \tag{12}$$

where absolute temperature T is in degrees Kelvin and the total pressure P is in atmospheres.

The dependence of carbon conversion on the CO_2/CO ratio and on temperature is shown in Fig. 19. Experimental rates are marked by circular (250°C), triangular (235°C), and square (225°C) symbols, and the theoretical kinetic curves using the integrated form of the above kinetic equation (11) with $m = 3$, $n = 3$, and $F = (1 + K_{H_2} p_{H_2} + K_{CO} p_{CO})$ are represented as solid lines passing through the experimental points. With this form of F the extent of adsorption of H_2O and CH_3OH is neglected; the effect of water and methanol is, however, taken into account by kinetic terms for the reverse reaction, but not for product desorption in the forward reaction. The set of constants with which best fits were obtained is given in Table IX for three cases: case I, as above, describing competition of CO, H_2, and CO_2 for sites A_{ox}; case II wherein CO are adsorbed on A_{ox} and H_2 competes with CO_2 for different sites; and case III wherein CO_2 competes with both CO and hydrogen, but CO and H_2 are adsorbed on different sites.

The statistical factors in the last column of Table IX show that all three models are nearly equally satisfactory. Thus the kinetic models appear to be insensitive to a specific mechanism by which CO and hydrogen utilize the catalyst sites in the synthesis. However, the promoting effect of CO_2 in creating the A_{ox} sites and the strong retardation of the synthesis by the adsorption of this gas had to be taken into account in all three cases. The kinetics case I may be regarded as a convolution of the original Natta kinetics with the general form describing the CO_2 effects in Eq. (11). It must be emphasized that Natta's kinetic model (*57*) was tailored for catalysts used at higher temperatures, while the model of Klier *et al.* (*56*) aimed primarily at a quantitative description of the low-temperature dependence

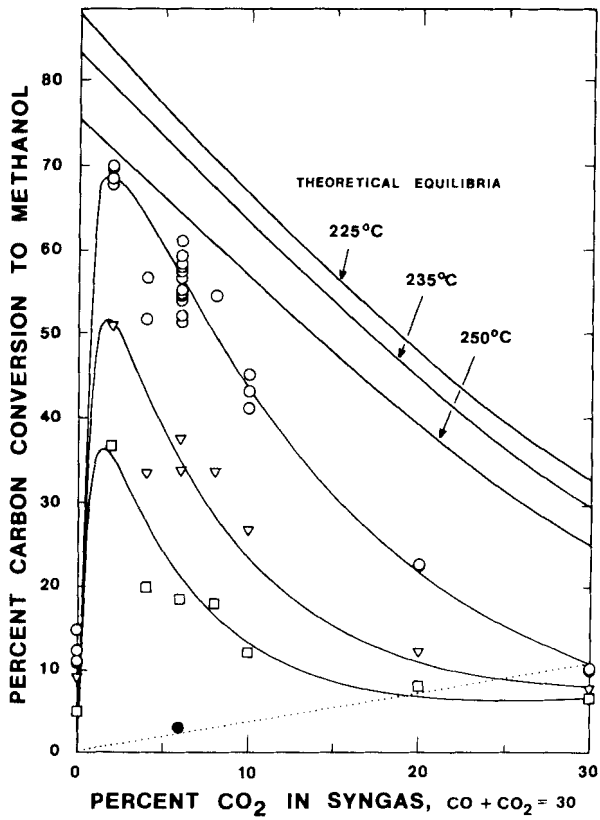

FIG. 19. The dependence of methanol synthesis rates at 225–250°C, 75 atm total pressure, and gas hourly space velocity 5000 hr^{-1} upon the ratio of concentrations of CO_2 and CO. The total hydrogen-to-carbon ratio in the feed gas was 7:3 for all CO_2/CO ratios. Experimental data are marked as open symbols and theoretical dependences, described by the kinetic model in text with the values of constants as in Table IX, as full curves. The closed symbol describes an equivalent of conversion rate when carbon dioxide in the mixture $CO/CO_2/H_2 = 24/6/70$ was replaced by argon (*56*). [Reprinted with permission from *J. Catal.*, **74**, 343 (1982). Copyright (1982) Academic Press, New York.]

of the synthesis on carbon dioxide pressure. Klier *et al.* considered adsorption of CO_2 dominant over that of methanol and incorporated the methanol-retarding terms only in the reverse reaction rates. This constitutes a major difference from Natta's treatment, and evidently the model can be refined.

Klier *et al.* further scrutinized their model to determine whether the temperature dependences of the various adsorption equilibrium constants would yield reasonable values of adsorption enthalpies and entropies. These thermodynamic entities, calculated from data in Table IX, are summarized

TABLE IX

Values of Constants Used for the Construction of Theoretical Dependences of Steady-State Carbon Conversions to Methanol upon the Percentage x of CO_2 in the Synthesis Gas of Composition $CO_2/CO/H_2 = x/(30 - x)/70$[a]

Case	Temp. (°C)	K_{CO}	K_{H_2}	K_{CO_2}	K'	kA_0^{3b}	k'^b	$K_{eq}{}^c$	$K'_{eq}{}^c$	Σ^2/n^d
I	225	12.52	1.77	39.62	158.2	1.064	2.18(−4)	9.034(−3)	9.237(−5)	0.0012
	235	8.58	1.40	21.52	125.4	1.253	2.70(−4)	5.409(−3)	6.573(−5)	
	250	5.00	1.00	9.00	90.0	1.584	3.75(−4)	2.625(−3)	4.095(−5)	
II	225	12.52	1.77	98.51	18.1	0.898	2.18(−4)	9.034(−3)	9.237(−5)	0.0016
	235	8.58	1.40	60.0	16.1	1.135	2.70(−4)	5.409(−3)	6.573(−5)	
	250	5.00	1.00	30.0	13.8	1.584	3.75(−4)	2.625(−3)	4.095(−5)	
III	225	12.52	1.77	19.8	79.1	0.088	2.18(−4)	9.034(−3)	9.237(−5)	0.0015
	235	8.58	1.40	10.8	62.7	0.120	2.70(−4)	5.409(−3)	6.573(−5)	
	250	5.00	1.00	4.5	45.0	0.195	3.75(−4)	2.625(−3)	4.095(−5)	

[a] A total pressure of 75 atm was maintained at all conversions (*56*).

[b] Rate constants per gram of catalyst per hour for rates expressed in moles of methanol per hour.

[c] Equilibrium constants for reactions $CO(g) + 2H_2(g) \rightleftharpoons CH_3OH(g)$ (K_{eq}) and $CO_2(g) + 3H_2(g) \rightleftharpoons CH_3OH(g) + H_2O(g)$ (K'_{eq}); K_{eq} and K'_{eq} are defined on p. 279.

[d] Sum of the squares of differences between theoretical and observed conversions for CO_2-containing synthesis gas mixtures divided by the number of measurements n.

in Table X along with the activation energies for the synthesis of methanol from CO (E_a) and from CO_2 (E'_a). In all cases the adsorption heats were found to be in the expected order $-\Delta H(CO_2) > -\Delta H(CO) > -\Delta H(H_2)$. Furthermore, the adsorption entropies had very reasonable values: $\Delta S(CO_2)$ corresponded to an entire (cases I and III) or very substantial (case II) loss of translational and rotational entropy of gaseous CO_2, 55.4 cal mol^{-1} deg^{-1}, while adsorbed CO and H_2 retained a significant portion of their gas-phase entropy (*56*). Thus the model that fits well the CO_2 dependence of the synthesis rate also provides a sound and attractive physicochemical picture of the synthesis: whereas CO and H_2 are bonded with intermediate strength and retain some mobility in the adsorbed phase, CO_2 appears relatively strongly bound and immobile. The behavior of CO and H_2 is favorable to the reaction in which carbon monoxide and hydrogen, adsorbed on different active centers, must meet in a reactive collision to form the product. At the same time, the strong immobile CO_2 adsorption points to the retarding effect of this gas at high CO_2/CO ratios, which is more pronounced and produces flatter plateaus on the methanol yield versus CO_2 concentration as the temperature decreases from 250 to 225°C. The retarding effect of CO_2 by its adsorption can also be seen from the residence times calculated from sorption entropies: at 235°C the CO_2 residence time, approximately 1 sec, is comparable with methanol turnover time, 11 sec, whereas the CO and H_2 residence times were estimated to have values between 10^{-7} and 10^{-9} sec (*56*). The latter finding justifies *a posteriori* the assumption of the model that the CO and H_2 adsorption equilibria are rapidly established. The long residence time of CO_2 indicates that the adsorption of this gas may not be at equilibrium at low temperatures, a fact that is reflected by observed slow attainment of steady state when going from low to high temperatures in CO_2-rich synthesis gas (*55*, *56*).

Evidently, the Cu/ZnO catalyst investigated in this work has a very good inherent activity for methanol but can be further improved for performance

TABLE X

Values of Activation Energies of Methanol Synthesis from Carbon Monoxide, $E_a(k)$, and from Carbon Dioxide, $E_a(k')$, and Adsorption Enthalpies ΔH and Entropies ΔS Derived from the Kinetic Model Utilizing Constants in Table IX[a]

	Case I	Case II	Case III		Case I	Case II	Case III
$\Delta E_a(k)$	8.23	11.74	16.53	$\Delta H(CO_2)$	−30.7	−24.6	−30.7
$\Delta E_a(k')$	11.28	11.28	11.28	$\Delta S(CO)$	−33.1	−33.1	−33.1
$\Delta H(CO)$	−19.0	−19.0	−19.0	$\Delta S(H_2)$	−22.6	−22.6	−22.6
$\Delta H(H_2)$	−11.8	−11.8	−11.8	$\Delta S(CO_2)$	−54.3	−40.3	−55.7

[a] 1 cal = 4.184 J; from Ref. *56*. Energies and enthalpies are in kcal/mol and entropies in cal mol^{-1} deg^{-1}.

in CO_2-rich synthesis gas by modifiers that weaken the adsorption energy of CO_2. A selection of such modifiers will be determined by the nature of sites that strongly adsorb CO_2. Such sites are more likely located on the zinc oxide surface than on copper metal surface and may be associated with the basicity of zinc oxide. Therefore it appears desirable to diminish the basicity of zinc oxide to achieve weaker bonding of CO_2. A specific model of basic sites for CO_2 that block sites that activate CO is shown below.

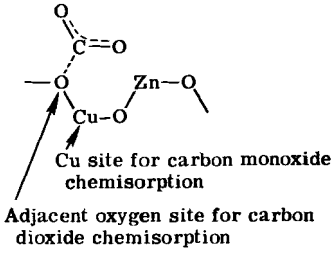

Once again the site involved in CO hydrogenation requires initimate interdispersion of copper and zinc oxide, which is consistent with the earlier conclusion that copper solute in zinc oxide is the catalytically active component.

In the kinetic treatment presented above it was necessary to postulate the active form of the catalyst to be its oxidized form A_{ox}, but it was not necessary to specify further what A_{ox} and A_{red} are chemically. In order to present a consistent picture of the catalyst formation and deactivation, Klier *et al.* (*56*) divided the redox equilibria between A_{red}, CO_2, A_{ox}, and CO into a reversible and an irreversible class, the latter giving rise to permanent deactivation of the catalyst. The reversible redox equilibria can be schematically represented as

$$CO_2 + \square_0 + 2e^- \rightleftharpoons CO + O^{2-}, \qquad Cu^+ + e^- \rightleftharpoons Cu_a^0, \qquad Zn^{2+} + e^- \rightleftharpoons Zn^+ \quad (13)$$

and also

$$CO_2 + H^-Cu^+ \rightleftharpoons CO + HO^-Cu^+$$

where $\square_0$ is a symbol for oxygen vacancy and Cu_a^0 for dispersed copper. The reduction of Cu^+ is considered predominant over that of Zn^{2+} at temperatures below 250°C.

The irreversible processes are segregation of copper, $Cu_a^0 \rightarrow$ Cu metal, and reduction to zinc and brass formation,

$$Zn^+ + e^- \rightarrow Zn, \qquad Zn + nCu \rightarrow Cu_nZn \quad (14)$$

both of which have been observed at high temperatures (*27*, *39*, *62*). Natta, however, noted that the reduction of zinc oxide is prevented by small amounts of water and carbon dioxide always present in the synthesis gas

(*10*), and so the most serious deactivation mechanism appears to be segregation of copper.

I. The Effect of Carbon Dioxide on Selectivity

Aside from the synthesis pattern shown in Fig. 19, carbon dioxide was found to cause amounts of methane to be formed at concentrations of CO_2 exceeding 10% in $(CO + CO_2)/H_2 = 30/70$ synthesis gas (*55*, *56*). Methane production increased with increasing concentration of CO_2 and with de-

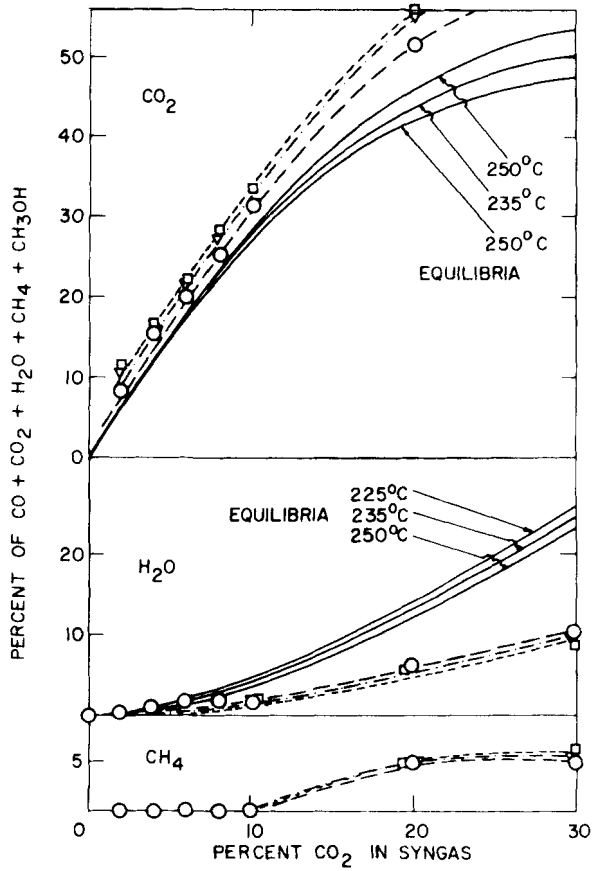

FIG. 20. The steady-state concentrations of carbon dioxide (top), water (center), and methane (bottom) as functions of the CO_2/CO ratio in the feed gas at 225–250°C, 75 atm total pressure, and GHSV 5000 hr^{-1} (*56*): (-○-) 250°C, (-·-▽-·-), 235°C, (-□-) 225°C. Conversions to methanol are given in Fig. 19. From Ref. *55*.

creasing temperature, as shown in Fig. 20 together with the steady-state concentrations of water and carbon dioxide. The latter behavior indicates that methane is formed from adsorbed CO_2. The pathway to methane must involve a direct hydrogenation of CO_2 and not a stepwise conversion of CO_2 to CO followed by hydrogenation of CO to methane, since in a CO-rich synthesis gas, methane is not a product.

J. Relative Hydrogenation Rates of Carbon Monoxide, Hydrocarbons, and Oxygenates

One of the useful methods of catalyst characterization is to compare rates of related reactions under similar pressure, temperature, and flow conditions. Furthermore, when carbon monoxide, another substrate, and hydrogen are allowed in contact with the catalyst simultaneously, their relative conversions reflect the extent to which these reactions components compete for the same active sites. Using the Cu/ZnO = 30/70 catalyst, the substrates carbon monoxide, 1-hexene, propionic acid, acrolein, propanaldehyde, benzene, toluene, and ethylbenzene were hydrogenated in vapor phase and in the presence of carbon dioxide under the pressure, temperature, and flow conditions at which CO is hydrogenated to methanol (*63*). The results are summarized in Table XI, which shows that the hydrogenation rates were substrate dependent in the order olefin > aldehyde > CO $\rightarrow$ CH_3OH > carboxylic acid > ethylbenzene $\approx$ toluene > benzene. A noteworthy observation is that methanol synthesis is a faster reaction than the aromatic ring hydrogenation over the Cu/ZnO catalyst, a pattern just opposite to that over methanation catalysts such as nickel (*64*). Vedage and Klier (*63*) further showed that carbon monoxide and other hydrogenable substrates compete for the same active sites. Their results, summarized in Table XII, demonstrate that all hydrogenable substrates suppress to varying degrees the rate of methanol synthesis from CO, and the presence of CO hinders to varying degrees the rate of hydrogenation of other substrates. Particularly interesting is the observation that the aromatic ring hydrogenation is completely stopped by the presence of CO, while methanol synthesis proceeds at a considerable rate in the presence of aromatics.

The relative hydrogenation rates of ethylbenzene, toluene, and benzene indicate that the aromatics are activated as π-donor complexes, the substituted benzenes being better donors than benzene. In view of the proposals identifying the active centers as Cu(I) species in the ZnO surface, it is beneficial to point out that Cu(I)/CO (*65*) and Cu(I)/olefin (*66*) complexes exist and that the Cu(I) species, free from the 4s screening electrons and being

TABLE XI

Relative Hydrogenation Rates of Carbon Monoxide, Hydrocarbons, and Oxygenates over the Cu/ZnO Catalyst[a]

Substrate	Conversion[b] (%)	Turnover rate[c] (sec^{-1})	Substrate feed rate (mol/hr)	Ionization potential (eV)
Benzene	16.6	4.95×10^{-3}	0.0068	9.24
Toluene	25	6.27×10^{-3}	0.0057	8.82
Ethylbenzene	29	6.24×10^{-3}	0.0049	8.76
Propionic acid	63	1.48×10^{-2}	0.0080	
Propanaldehyde	99	4.23×10^{-1}	0.29	
1-Hexene	100	4.33×10^{-1}	0.30	
Carbon monoxide	55	2.96×10^{-1}	0.147	

[a] Cu/ZnO = 30/70 catalyst described in Ref. *39*. The hydrogenation products were saturated hydrocarbons in the case of aromatics and the olefin, primary alcohols in the case of oxygenates, and methanol in the case of CO. From Ref. *63*.

[b] Conversion measured at 250°C, 75 atm, over 2.45 g catalyst using a feed of 10.5 liters (STP) of hydrogen per hour (0.43 mol H_2/hr) and that of the substrate indicated in the fourth column of this table.

[c] The turnover rate was calculated from the measured conversion rates assuming 2×10^{18} sites/m^2 of ZnO on the Cu/ZnO catalyst having 23.3 m^2 ZnO surface per gram of catalyst (*43*). The turnover rate is defined as number of conversions per site per second per hydrogen molecule consumed. Hence the substrate turnover is two (three) times smaller in the case where the substrate is hydrogenated by two (three) hydrogen molecules.

TABLE XII

Hydrogenation Rates of Carbon Monoxide, Hydrocarbons, and Oxygenates When CO Plus an Additional Substrate and Hydrogen Were Admitted to the Cu/ZnO Catalyst[a]

Reaction mixture[b]	Amounts of substituents	MeOH (%)	Other product (%)
$CO/CO_2/H_2$	24/6/70	55	—
1-Hexene/$CO/CO_2/H_2$	4.4/22.9/5.8/66.8	25–42[a]	100 *n*-Hexane
Propanaldehyde/$CO/CO_2/H_2$	3.9/23/5.8/67.2	32–51[a]	99 *n*-Propanol
Acrolein/$CO/CO_2/H_2$	1.5/23.6/5.9/69.0	13.6[a]	99 *n*-Propanol
Propionic acid/$CO/CO_2/H_2$	1.3/23.7/6.0/69.0	0.6[a]	63 *n*-Propanol
Ethylbenzene/$CO/CO_2/H_2$	0.8/23.8/6.0/69.4	31.5[a]	Traces of toluene
Toluene/$CO/CO_2/H_2$	0.9/23.8/6.0/69.3	34.0[a]	0
Benzene/$CO/CO_2/H_2$	1.1/23.7/6.0/69.2	30.5[a]	0

[a] See Table XI footnotes.

[b] The $CO/CO_2/H_2$ = 24/6/70 mixture was used at 250°C, 75 atm, and total flow rate of 15 liters/hr over 2.45 g of the Cu/ZnO = 30/70 catalyst. The substrate was admitted from a liquid feed valve to produce concentrations indicated in the first column.

good "two-way acceptors," are better suited for binding carbon monoxide and unsaturated organic compounds than any other valence states of copper (*67*).

VI. Other Binary Catalysts

There are several metal–oxide combinations other than the Cu/ZnO that have been reported active in methanol synthesis at low temperatures and pressures. These can be divided into catalysts containing copper and an oxide and catalysts containing a transition metal and an oxide.

A. Copper-Based Catalysts

One of the recently studied catalysts is the copper–thoria composite made by oxidation and subsequent reduction of copper–thorium intermetallics such as Th_2Cu, $ThCu_2$, $ThCu_{3.6}$, and $ThCu_6$. Baglin *et al.* (*68*) found that air oxidation caused the alloy elements to segregate into a heterophase thoria, copper, and copper oxide mixture and that subsequent reduction in hydrogen or in the synthesis gas produced a catalyst containing crystalline copper and thoria. Catalysts with surface areas in the range 25–50 m^2/g were made in this manner.

Baglin *et al.* also stated, quoting Herman *et al.* (*39*), that the absence of diffraction lines of copper oxides would not preclude the presence of Cu(I) or Cu(II) in the reduced catalysts and noted that further characterization of the copper–thoria catalyst may prove illuminating. The results of testing of this catalyst at 220–300°C, 60 atm, H_2/CO ratio equal to 16/1, and space velocity 31,000 hr^{-1} are summarized in Table XIII. The reported methanol conversions were high, and the yields at 260°C were comparable to those of the Cu/ZnO catalysts tested at 250°C, 75 atm, H_2/CO ratio 3/1, and space velocity 5000 hr^{-1}: the $Cu/ThO_2 = 5/1$ catalyst yielded 0.995 kg methanol per liter of catalyst per hour (*68*), while the Cu/ZnO = 30/70 catalyst yielded 1.10 kg methanol per liter of catalyst per hour (*39*) under the stated conditions. Table XIII also shows products other than methanol, i.e., methane, ethylene, dimethylether, CO_2, and water that were formed over the Cu/ThO_2 catalyst. The selectivity of the Cu/ThO_2 catalyst for methanol was good but not as high as that of the Cu/ZnO catalyst, the main side product being methane. A major difference appears to be that high conversions are obtained with the Cu/ThO_2 catalyst in a CO_2-free synthesis gas, while the presence of CO_2 was necessary for maximizing the activity of the Cu/ZnO catalysts. The activity of the Cu/ThO_2 catalyst was found to decrease at

TABLE XIII

Gaseous Product Analysis as a Function of Temperature from the Synthesis of Methanol over $ThCu_{3.6}$, Preactivated in Air[a]

Temp. (°C)	Mol % excluding H_2							Yield of CH_3OH (kg/liter catalyst hr^{-1})[b]
	CO	CH_4	CO_2	C_2H_6	H_2O	CH_3OH	$(CH_3)_2O$	
220	83.52	0.24	0.08			16.16		0.386
240	67.22	0.60	0.28			31.89		0.761
260	55.93	1.24	1.07	0.06		41.70		0.995
270	52.26	1.99	1.58	0.08	0.56	43.54		1.039
280	49.42	2.85	2.46	0.13	1.11	44.02		1.050
300	54.44	5.49	3.65	0.17	1.91	34.04	0.31	0.812

[a] At 400°C; $16H_2$: CO; 60 atm pressure; 31,000 gas hourly space velocity; according to Baglin *et al.* (*68*).

[b] Calculated by the present author.

2–2.5%/day in a test involving 161 hr on stream. The catalyst performance was compared with that of a commercial $Cu/ZnO/Al_2O_3$ catalyst (United Catalysts, Inc., C79-4) under identical reaction conditions and the yields were found to be 6.7 times higher over the Cu/ThO_2 catalyst. The activity of the Cu/ThO_2 catalyst could not be correlated with the total BET surface areas or with areas determined by chemisorption of carbon monoxide. The authors also stated that no standard method to measure the surface area of copper catalysts exists, an opinion based on a report by Scholten and Konvalinka (*69*) but which is at variance with those of Andrew (*27*), Parris and Klier (*43*), and literature cited in these two latter reports. It is evident that the Cu/ThO_2 catalysts are good prospects and due for a detailed characterization study. However, the claim that they are significantly more active than commercial $Cu/ZnO/Al_2O_3$ catalysts is not substantiated because the best industrial catalysts based on this composition give yields higher than those reported for Cu/ThO_2 under comparable conditions (compare Tables XIII and I).

Aside from the recently described Cu/ThO_2 catalysts, copper on chromia and copper on silica have been reported to catalyze methanol synthesis at low temperatures and pressures in various communications that are neither patents nor refereed publications. It is not feasible to critically review statements unsupported by published data or verifiable examples. However, physical and chemical interactions similar to those documented in the copper–zinc oxide catalysts are possible in several copper–metal oxide systems and the active form of copper may be stabilized by oxides of zinc, thorium, chromium, silicon, and many other elements. At the same time it is doubtful that more active and selective binary copper-based catalysts than

the optimized Cu/ZnO composites will be found, since the components of the latter seem to be ideally suited for the mutual synergic promotion required for the low-temperature methanol synthesis.

B. Transition-Metal-Based Catalysts

Among the transition metals, Pd, Pt, Ir, and Rh in various forms have been reported active in methanol synthesis (*32–34*), as noted in Section II. Palladium, platinum, and iridium metals were supported on silica, and it has recently been suggested that palladium is present in its valence state Pd(II) which is the active form of the catalyst (*70*). Under the synthesis conditions the Pd(II) ions could not survive the highly reducing atmosphere of the CO/H_2 synthesis gas, and so this valence state would have to be induced by the presence of silicon dioxide. Should this be a general case, silica would not act merely as an inert support, and the silica-supported transition metals would have to be considered binary catalysts whose active state is formed by a "support–metal interaction."

A dramatic effect of the support has been reported by Ichikawa (*33*, *71*, *72*) for rhodium catalysts prepared by deposition and thermal decomposition of multinuclear rhodium carbonyls on various oxides. When zinc oxide or magnesium oxide were used as supports, methanol was the predominant product. On the other hand, rhodium supported on titania or lanthana gave ethanol as major product, and rhodium on silica or γ-alumina yielded hydrocarbons. These experiments were carried out at subatmospheric pressure and the yields of methanol were very low. In addition, methane was a significant by-product, as demonstrated in Fig. 21. In a subsequent communication Ichikawa reported higher yields and selectivities when the synthesis was carried out at higher pressures (*72*). Methanol and methane were also formed over a catalyst comprising rhodium and lanthanum hexaboride (*73*). In order to compare the activity of Rh/LaB_6 with those of Rh/ZnO and Rh/MgO, published by Ichikawa, the former was prepared in the author's laboratory by a deposition of 0.1 g of $Rh_4(CO)_{12}$ from tetrahydrofuran (THF) solution onto 20 g of LaB_6 support (14.5 m^2/g), followed by evaporation of THF and thermal decomposition of the rhodium carbonyl at 180°C in nitrogen. The resulting catalyst was tested at 75 atm in the temperature range 200–275°C with the synthesis gas $CO/CO_2/H_2 = 24/6/70$; methanol and methane were the only carbon-containing products with yields given, along with those over the Pd/SiO_2, Rh/MgO, and $Rh/Fe/SiO_2$ catalysts noted in Table XIV. A comparison of these yields with those over the Cu/ZnO catalysts demonstrates that the rhodium-based catalysts are inferior to the copper–zinc oxide catalysts on the basis of both the catalyst total volume

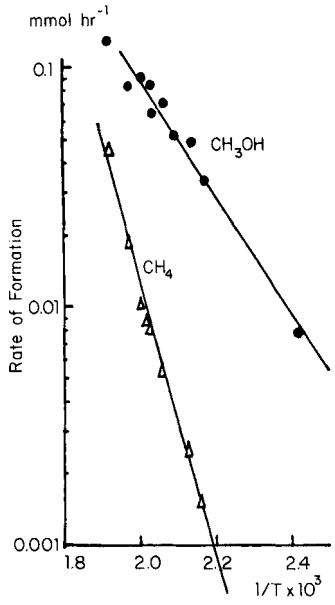

FIG. 21. Arrhenius plots of methanol and methane formation over the pyrolyzed catalyst on MgO prepared from $Rh_4(CO)_{12}$ 0.11 g (0.15 mmol) and MgO 20 g, 0.75% Rh wt. dispersion. The reactor volume was 320 ml; $CO:H_2 = 200$ Torr:450 Torr (*33*). [Reprinted with permission from *Bull. Chem. Soc. Jpn.* **51**, 2268 (1978). Copyright 1978 Chemical Society, Japan.]

and the weight of the rhodium metal. Although the reaction conditions are not quite compatible, the results indicate that the activity of the palladium–silica catalysts are intermediate between Cu/ZnO and Rh/MgO or Rh/LaB_6. The silica-supported platinum and iridium catalysts had activity lower than the Pd/SiO_2 catalysts (*32*).

In the effort to modify the catalytic properties of rhodium, Wilson and co-workers prepared $Rh/Fe/SiO_2$ and other two-metal–silica combinations (*74*); methanol yields over a $Rh/Fe/SiO_2$ catalyst shown in Table XIV were higher than those over the Rh/MgO, Rh/ZnO, and Rh/LaB_6 catalysts prepared from cluster carbonyls, but the selectivity of the latter toward methanol was better than that of bimetallic rhodium–iron catalysts.

In the absence of a detailed characterization of the supported rhodium, it is premature but nevertheless interesting to speculate about which property of the oxide "support" induces methanol synthesis activity in small rhodium particles. The effects that might be involved here are acid–base or electron transfer interactions between the support and the rhodium particles, including the change of the effective valence state of rhodium. Basic oxides such as ZnO or MgO will tend to donate electron pairs to the rhodium

TABLE XIV
Supported Transition-Metal Catalysts for Methanol: A Comparison of Activities

Catalyst composition	Reactants	Temp. (°C)	Pressure (atm)	Yield (kg liter^{-1} hr^{-1})	Reference
Pd/SiO_2	$H_2 + CO$	350	100	0.23[a]	*32*
Rh/MgO	$H_2 + CO$	250	0.85	0.0002[a]	*33*
				0.07[b]	*33*
				0.00015[c]	*33*
				0.05[c]	*33*
Rh/LaB_6	$H_2 + CO$	250	75	0.004[a]	*73*
				0.15[b]	*73*
				0.0044[c]	*73*
				0.19[d]	*73*
$Rh/Fe/SiO_2$	$H_2 + CO$	300	68	0.02[a]	*34, 74*
				0.06[e]	*34, 74*

[a] Methanol yield in kg/liter catalyst hr^{-1}.
[b] Yield of methanol in kg/kg Rh hr^{-1}.
[c] Methane yield in kg/liter catalyst hr^{-1}.
[d] Methane yield in kg/kg Rh hr^{-1}.
[e] Yield of $CH_4 + CH_3OH + C_2H_5OH + C_2$ chemicals and oils.

particles to fill some of its d levels and possibly produce effective electron configurations of the metal closer to one on the right-hand side in the periodic table, i.e., to palladium. Such an electron transfer or polarization will have the effect of suppressing carbon monoxide dissociation on the metal and will amount to crossing the division line between hydrocarbon and methanol synthesis catalysts in Table III from the left to the right (*75*). In order for the basic support–metal interactions outlined above to be effective in modifying the chemical properties of the metal, it is imperative that the metal particles be very small. Although the catalyst preparation by decomposition of carbonyls is designed to produce very small metal clusters, there is a suspicion that these clusters may agglomerate during use. Therefore, any rational explanation of support effects in the rhodium catalysis must await a detailed characterization of the metal dispersion.

VII. Ternary and Quaternary Catalysts

Ternary compositions $Cu/ZnO/Al_2O_3$ and $Cu/ZnO/Cr_2O_3$ are currently the most important industrial catalysts. The solid-state chemistry of these composites is often complex, but there is no evidence that addition of alumina or chromia to the binary Cu/ZnO systems causes significant synergic

promotion. Other third components, however, are known to alter the selectivity of the Cu/ZnO catalysts and in some cases act as retardants through a great number of possible solid-state reactions which perturb the delicate balance of copper in zinc oxide that is necessary for the catalyst formation. In this section we shall concentrate on the "structural promotion" by alumina and by various products of its interaction with zinc oxide and copper. There are many preparations and different ratios of copper, zinc oxide, and alumina, or chromia that result in successful catalysts, as is apparent from Tables I and II and the literature quoted therein. Two types of these "formulations" were characterized better than others, and these are discussed in some detail.

ICI catalysts contain deliberate additions of crystalline zinc aluminate spinel $ZnAl_2O_4$. Andrew (*27*) stressed the importance of this refractory oxide in stabilizing the catalyst for long-term performance. The ICI catalyst was reported to be a mixture of microcrystalline copper of average particle size between 5 and 7 nm, microcrystalline zinc aluminate, and perhaps also zinc oxide. One of the functions of zinc aluminate was suggested to be to maintain the copper particles in fine dispersion, and data from ICI plants were analyzed under the assumption that the surface of the copper crystallites was the catalytically active part of the composite (*27*). The ICI $Cu/ZnAl_2O_4/ZnO$ catalysts exhibited dependence on the CO_2/CO concentration ratio similar to the binary Cu/ZnO catalysts described by Klier *et al.* (*56*). The catalysts were severely deactivated in CO_2-free synthesis gas, an effect attributed by Andrew to the reduction of zinc oxide with the concomitant alloying of zinc with copper. This would be the more severe mode of deactivation, grouped among the irreversible processes [Eq. (13)]. In principle, the CO_2/CO dependence of the synthesis rates over the ICI catalysts can be described by the same formal kinetics as presented for the Cu/ZnO binaries on p. 279. Both sets of data require the reduced form of the catalyst A_{red} to be inactive, despite the disagreement on what is the chemical nature of A_{red} at low temperatures: Andrew's proposal is that A_{red} is brass and A_{ox} is metallic copper, while the Klier *et al.* basic concept is that A_{red} is metallic copper and A_{ox} is monovalent copper in zinc oxide. It appears likely that the same set of solid-state reactions underlies the observed CO_2/CO dependences over the ternary $Cu/ZnAl_2O_4/ZnO$ and the binary Cu/ZnO catalysts, no matter which interpretation of the chemical nature of the redox process involved in the formation of A_{ox} will eventually prevail.

Another type of preparation of the $Cu/ZnO/Al_2O_3$ catalyst involves coprecipitation of the three components and the resulting catalyst contains neither spinel nor crystalline alumina. Fischer *et al.* (*76*) reported that a ternary catalyst of the nominal composition $Cu/ZnO/Al_2O_3 = 60/35/5$ mol% contained only crystalline copper and zinc oxide, and all the alumina

was in X-ray amorphous form. The chemical composition and the amounts of X-ray crystalline matter are given in Table XV. The error given for the crystallinity, $\pm 10\%$, was too large to determine whether any part of zinc oxide or copper was X-ray amorphous, but the chemical Cu/ZnO ratio (1.7) was substantially greater than the average X-ray crystallinity Cu/ZnO ratio (1.38). It is interesting to note that were all ZnO crystalline as in the binary Cu/ZnO catalysts (see Fig. 5), the comparison of the chemical and crystalline Cu/ZnO ratio would indicate 19% of the copper to be X-ray amorphous. Consequently, the mole ratio of X-ray amorphous copper to zinc oxide would be 0.4, exceeding that found by Bulko *et al.* (*41*) in the binary Cu/ZnO catalysts.

Further evidence that part of copper is X-ray amorphous in the ternary catalysts follows from the work of Herman *et al.* (*77*). These authors prepared a $Cu/ZnO/Al_2O_3 = 60/30/10$ catalyst by coprecipitation of a precursor from the solution of Cu^{2+}, Zn^{2+}, and Al^{3+} acetates by sodium carbonate, washing, calcination at 350°C, and reduction at conditions identical with those employed for the preparation of Cu/ZnO composites. The resulting catalyst consisted of particles shown in Fig. 22a. The large hexagonal particles had a structure of a single-crystal wurtzite zinc oxide oriented with its sixfold axis perpendicular to the hexagonal plane outline of the crystal, as documented by the diffraction pattern in Fig. 22b. The analysis in the STEM showed that this type of particle contained 8 at.% Cu, 50 at.% Zn, and 42 at.% Al. Separate large copper crystallites, showing as dark areas in the electron micrograph of Fig. 22a, were also constituents of the catalyst, but their surface area was estimated to be negligible compared to that of the porous ZnO platelets. Given the earlier result that large-particle crystalline copper does not catalyze methanol synthesis, the activity of this catalyst resides in the "micromonolith" porous particle of ZnO that contains all three elements Cu, Zn, and Al. Interestingly enough the pore walls, which are perpendicular to the platelet major dimension, expose the same prism plane of zinc oxide as the most active binary catalyst Cu/ZnO = 30/70, and very likely the chemical and physical nature of the active surface

TABLE XV

Chemical Composition and X-ray Crystallinity of Cu/Zn/Al Oxide Catalyst[a]

Catalyst composition[b] (Cu/Zn/Al) (at. %) determined	
(1) chemically, 60/35/5	(2) X-ray diffraction ($\pm 10\%$), 58/42/0

[a] According to Fischer *et al.* (*76*).

[b] Technical low-pressure methanol catalyst prepared by coprecipitation and reduced at 240°C.

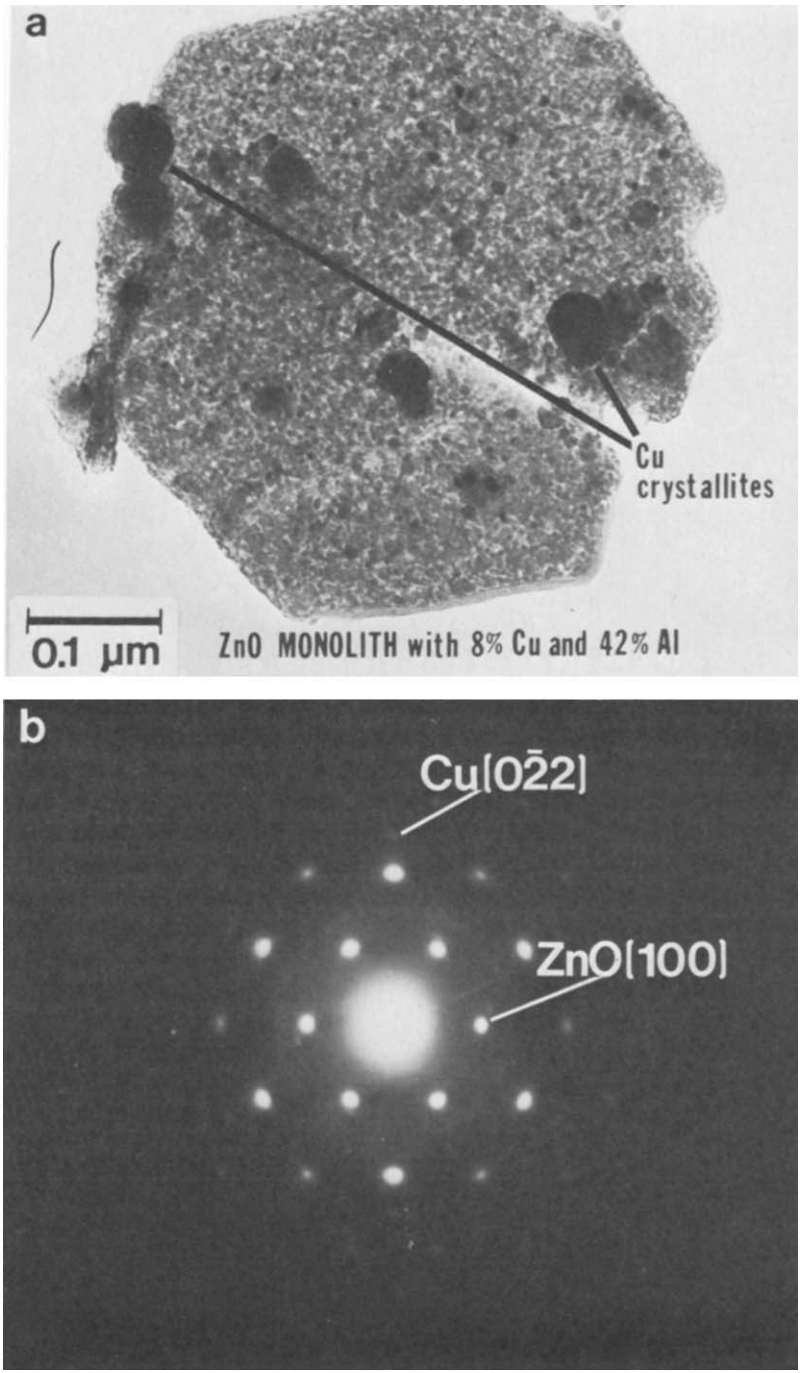

FIG. 22. (a) Transmission electron micrograph and (b) selected area diffraction pattern of a single hexagonal porous particle of the $Cu/ZnO/Al_2O_3$ catalyst prepared from acetates (77). The Cu/Zn/Al ratio exclusive of crystalline copper, which appears as dark crystallites, was equal to 8/50/42.

of the two catalysts is identical. Herman *et al.* (*77*) suggested that the role of amorphous alumina is to "glue" the zinc oxide microcrystals doped with amorphous copper solute around the 5-nm pores. The specific activity for methanol of this $Cu/ZnO/Al_2O_3$ catalyst was nearly equal to that of the binary Cu/ZnO = 30/70 catalyst, so that the effect of alumina appears to be structural promotion only.

A different view on the role of amorphous alumina was taken by Fischer *et al.* (*76*). These authors noted that copper in the ternary $Cu/ZnO/Al_2O_3$ catalysts displayed paracrystallinity, i.e., a defect crystalline state in which long-range order may be perturbed by "endotactic" inclusions—randomly distributed species whose dimensions have a strong misfit with the host lattice of the copper crystallites. Fischer *et al.* argued that these endotactic inclusions are small Al_2O_3 clusters because no crystalline alumina could be found in the catalyst. The effect of inclusions was suggested to be indirect: the lattice disorder would cause some of the surface copper atoms to be displaced from their lattice positions, which then bind carbon monoxide with a different strength than the lattice atoms. Quantum mechanical calculations have predicted that the atoms displaced only 10% from their lattice positions would bind CO more weakly than atoms in ideal lattice positions, and Fischer *et al.* further argued that this weaker form of CO, because of its greater mobility, would be one that is most rapidly hydrogenated to methanol. This concept is in contrast to the observations of Parris and Klier (*43*) who found an irreversibly bonded type of carbon monoxide on the more active of the binary catalysts (see Fig. 13) and concluded that the hydrogenable form is the more strongly adsorbed CO on the solute copper centers in zinc oxide. In neither case is the catalyst activity expected to be proportional to the copper metal surface area: the density of defects induced by inclusions will depend more on the nature and concentration of the inclusions, and the density of copper solute atoms will depend more on chemical interactions between the copper and the host lattice than simply on the copper surface area. A comparison of activities of the Cu/ZnO catalysts and the $Cu/ZnO/Al_2O_3$ catalyst prepared by Herman *et al.* (*77*) indicates that the presence of alumina did not bring about a dramatic change of specific activity. It is therefore concluded that paracrystallinity due to alumina inclusions was not a significant determinant of activity of the latter catalyst.

In summary, several roles were attributed to alumina in the $Cu/ZnO/Al_2O_3$ catalysts: prevention of copper particle sintering through the formation of zinc aluminate, induction of surface defects by endotactic inclusion of alumina clusters in copper, and that of stabilization of highly dispersed Cu/ZnO binary catalyst. It is possible that all these effects take place in varying degrees in the commercial catalysts, but there is no evidence at this time that the specific activity of the present commercial catalysts Cu/ZnO/

Al_2O_3 catalysts originates from interactions other than those existing in the binary system Cu/ZnO. The structural promotion by alumina is a very significant factor in the formulation of industrial catalysts, however, as it imparts chemical and mechanical stability required for a long-lived catalyst in large-scale reactors.

It is noteworthy that components other than alumina often have detrimental chemical and physical effects on the catalyst. For example, Herman *et al.* (*77*) reported that addition of ceria to the Cu/ZnO catalyst lowered methanol conversion by a factor of 5, despite the presence of a large concentration of microparticulate copper metal. This effect was explained by the ability of ceria to drive copper from the active state in zinc oxide solution to inactive metallic copper. Chromia, which had been used as a component of catalysts for methanol for a considerable period of time, is a suitable structural promoter, but some preparations result in an increase of concentration of side products such as higher alcohols (*39*), dimethyl ether (*47*), or even hydrocarbons.

There are other components such as alkali, transition metals cobalt and rhodium, oxides of iron, manganese, vanadium, and rare earths, which have at one time or another been used in combination with copper and zinc oxide. The effects of alkali and cobalt metal are to lower the selectivity to methanol with a significant coproduction of hydrocarbons and higher alcohols. Recently a quaternary catalyst has been patented (*78–80*), based on a combination of copper, cobalt, transition-metal oxide, and alkali oxide that produced from the synthesis gas a mixture of C_1–C_4 alcohols with the major product being ethanol. This catalyst contains components of methanol catalysts and components of Fischer–Tropsch or homologation catalysts. The process is being evaluated as of the time of this writing. The reported product composition and yields over this and other recently reported catalysts that have produced significant amounts of low alcohols have been summarized by Klier (*75*). The claimed activities of the copper–cobalt–transition oxide–alkali catalysts are higher than those of the rhodium-based catalysts. The understanding of the function of these catalysts must await detailed characterization of the structural, electronic, and morphologic properties of their components, similar to the one achieved with the simpler Cu/ZnO methanol catalysts.

VIII. Mechanisms

Kinetic experiments performed by Natta *et al.* (*57*) with a ZnO/Cr_2O_3 catalyst and by Klier *et al.* (*56*) with the Cu/ZnO = 30/70 catalyst, as well as the high-power dependence of the synthesis rate on the concentration of

active sites measured by irreversible CO chemisorption (Fig. 17) and on reactant pressures (Fig. 18), indicate that each molecular synthesis step requires several sites. Natta stressed that kinetic equations, based on the hypothesis that the surface reaction is bimolecular, did not fit the observed rate dependences on the partial pressures of the reaction components. Only with the hypothesis of a trimolecular surface reaction involving one CO and two H_2 adsorbed molecules was it possible to interpret the rates observed over the ZnO/Cr_2O_3 catalyst quantitatively. Later developments have shown that several kinetic models will fit Natta's original data, but a common feature to all was that the synthesis rate depended on positive powers of partial pressure of hydrogen and carbon monoxide, the dependence on hydrogen being stronger than that on carbon monoxide. Klier *et al.* (*56*) also treated the synthesis over the low-temperature Cu/ZnO catalyst as a trimolecular surface reaction and obtained a successful kinetic model.

Mechanistic interpretation of the kinetic models may be as follows. Equilibria of carbon monoxide and molecular hydrogen between the gaseous phase and adsorbate are rapidly established. While the CO and H_2 molecules undergo dynamic exchange between the gas and adsorbed phase and among the surface sites, a small fraction of each, proportional to their surface concentrations, is activated for a reactive collision. The activation may involve splitting of hydrogen molecules into atoms, and partially hydrogenated species may include formyl HCO, formaldehyde HCHO, hydroxycarbene HCOH, hydroxymethyl CH_2OH, and methoxyl CH_3O. With the participation of oxygen atoms of the solid oxide, of carbon dioxide, or water, formate $HCOO^-$ is also a possible intermediate. Once the reactive collision has occurred, the subsequent partial reactions are irreversible and rapid. For this reason, the kinetically significant intermediates are difficult to detect during the synthesis by either physical or chemical methods, and consequently the synthesis mechanism has not been firmly established. Yet it is very important to understand some fundamental features of the synthesis pathway because knowledge of mechanistic details will allow the control of selectivity to side products, where desirable, and pave the way for the design of catalysts for alkylations with the synthesis gas and other related reactions.

A. Possible Reaction Pathways

The mechanisms proposed in the past may be divided into three basic groups: carbon-down, represented by the sequence

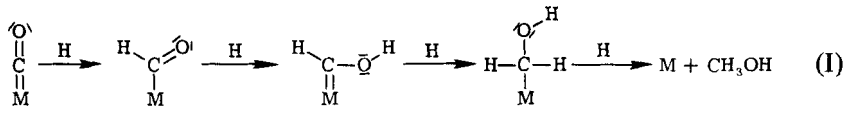

(I)

oxygen-down, represented by the sequence

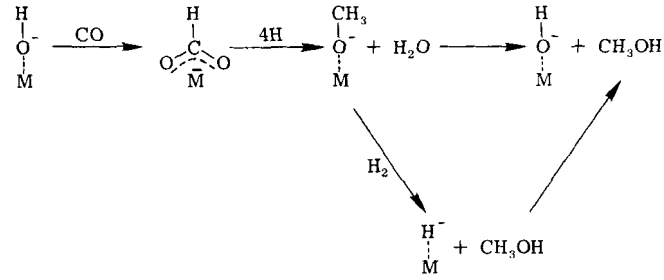

(II)

and side-on hydrogenation

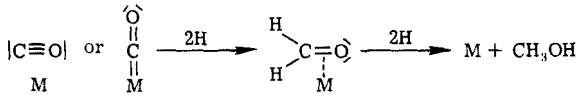

(III)

Here M is a symbol for a site involved in the activation of carbon monoxide.

It is helpful to summarize briefly the thermodynamic energies of the various intermediates in pathways I–III. Figure 23 shows enthalpies and Gibbs free energies at 250°C which would be required for noncatalyzed reactions that involve a particular set of intermediates. Pathway II is drawn in Fig. 23 for potassium hydroxide, formate, methoxide, and hydride because of the lack of available thermodynamic data for the corresponding compounds of zinc and copper. Nevertheless, the relative values of ΔG and ΔH illustrate the points to be made. The role of the catalyst for Scheme I would be to lower the 200 kJ/mol thermodynamic barrier by suitable bonding of hydroxycarbene HCOH, while pathway II would require destabilization of the surface formate and methoxide. It is also seen that the removal of surface methoxide by hydrolysis would proceed with a lower thermodynamic barrier than by hydrogenation. Pathway III would seem to be a feasible one because the free energy of formaldehyde lies only 17 kJ/mol above that of methanol. However, formaldehyde has never been observed as intermediate in methanol synthesis over catalysts reviewed here. On the other hand, formaldehyde was frequently found to be the product of methanol decomposition (*9*, *81–83*). It is therefore likely that large kinetic barriers exist for the synthesis of formaldehyde that offset the thermodynamic feasibility of pathway III. It is evident that entirely different requirements would be imposed on catalysts for pathways I, II, or III: route I would require stabilization of hydroxycarbene, route II destabilization of formate and methoxide, and route III lowering of the kinetic barrier for formaldehyde synthesis. In the effort to detect some of the intermediates listed in Fig. 23, various workers in the field resorted to experimental

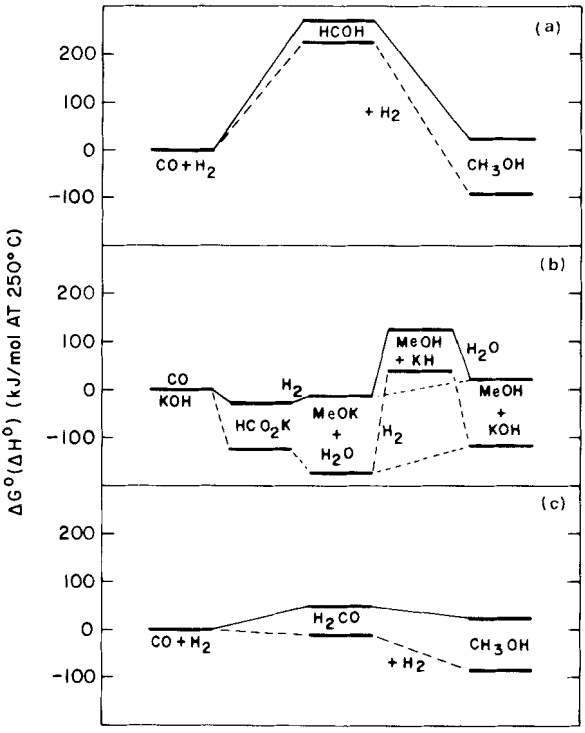

FIG. 23. Standard enthalpy (dashed lines) and Gibbs free-energy (full lines) changes for intermediates in methanol synthesis.

(a) Pathway I: hydroxycarbene route

$$CO(g) + H_2(g) \rightarrow HCOH(g), \qquad HCOH(g) + H_2(g) \rightarrow CH_3OH(g)$$

(b) Pathway II: formate–methoxide route

$$CO(g) + KOH(s) \rightarrow HCOOK(s)$$
$$HCOOK(s) + 2H_2(g) \rightarrow CH_3OK(s) + H_2O(g)$$
$$CH_3OK(s) + H_2(g) \rightarrow CH_3OH(g) + KH(s)$$
$$CH_3OK(s) + H_2O(g) \rightarrow CH_3OH(g) + KOH(s)$$

(c) Pathway III: formaldehyde route

$$CO(g) + H_2(g) \rightarrow H_2CO(g), \qquad H_2CO(g) + H_2(g) \rightarrow CH_3OH(g).$$

methods, outlined below, which gave partial insight into the methanol synthesis mechanisms.

B. Methods Used in Mechanistic Studies of Methanol Synthesis

Chemical composition of side products of methanol synthesis and decomposition has often been reported but rarely used for the resolution of

mechanism. The most frequent side products in the synthesis, when run over less than optimally selective catalysts, are dimethylether, higher alcohols, methane, and methyl formate. While dimethylether and higher alcohols are clearly products of secondary reactions, methane and methyl formate may be formed directly from the surface intermediates containing one carbon atom. The presence of methane is diagnostic of the C—O bond cleavage, as discussed in Section V,I. Methyl formate may be formed by a number of reactions; among others, thermodynamic driving forces exist in favor of esterification

$$HCOOH(g) + CH_3OH(g) \rightleftharpoons HCOOCH_3(g) + H_2O(g) \tag{15}$$

where $\Delta H_{250^\circ C} = -9.54$ kJ/mol, $\Delta G_{250^\circ C} = -13.39$ kJ/mol, and of disproportionation of formaldehyde

$$2HCHO(g) \rightleftharpoons HCOOCH_3(g) \tag{16}$$

where $\Delta H_{250^\circ C} = -116.44$ kJ/mol, $\Delta G_{250^\circ C} = -46.77$ kJ/mol. If related reactions take place on the catalyst surface, then perhaps methyl formate could be formed from surface formate, methoxide, or formyl residues. It is interesting to note that in an early study of methanol decomposition over the Cu/ZnO catalysts, Frolich *et al.* (*6*) found methyl formate and formaldehyde to be the predominant products over the copper-rich composites, including copper metal, whereas carbon monoxide was the dominant product over the zinc-oxide-rich catalysts. While the decomposition rates to carbon monoxide paralleled those of methanol synthesis rates (*6*), there was no correlation between the decomposition of methanol to methyl formate and the synthesis. Since methyl formate was also formed over pure copper, the oxygen of an oxide does not appear to be necessary for the occurrence of methyl formate. Consequently the presence of methyl formate, either in the synthesis or in the decomposition of methanol is not unambiguous evidence for pathway II with surface formate being an intermediate.

Coadsorption of reactants and subsequent *thermal decomposition* of the surface complexes formed have been used to resolve the mechanisms in several studies (*81–84*). Mutual enhancement of the adsorbed amounts of the reactants is indicative of their interaction, and if the adsorption of separately admitted components is negligible, the stoichiometry of the adsorbed complex can be determined. Further evidence for the formation of an adsorbed complex, employed in a mechanistic study of methanol synthesis over ZnO (*84*), is obtained by thermal decomposition of the adsorbed complex: if the reactants appear simultaneously at one temperature upon thermal desorption from a coadsorbed layer, but if each reactant adsorbed separately gives a thermal desorption peak at a different temperature, the existence, although not necessarily the structure or com-

position, of the adsorbed complex has been clearly established. *Isotope methods* can also be used for the determination of certain features of the methanol synthesis mechanism. If the carbon monoxide is initially mixed from $^{13}C^{16}O$ and $^{12}C^{18}O$ and if the methanol product contains no $^{13}CH_3{}^{18}OH$ and $^{12}CH_3{}^{16}OH$, it can be concluded that (1) C—O bond does not rupture and (2) the synthesis does not proceed via formate with the participation of oxygen of an oxide or other sources such as CO_2 or water. Clearly, a rapid shift reaction or exchange reactions of the catalyst oxygen with CO would scramble ^{13}C and ^{18}O between CO, CO_2, and water, and would preclude the above result. In one experiment hydrogen in the synthesis gas was rapidly replaced by deuterium, and CH_3OD was found to be predominant product (*85*). Such an isotope composition of the product would prove that the slow hydrogenation is that of a CH_3O intermediate, if it were proven simultaneously that CH_3OH methanol does not rapidly exchange its hydroxylic hydrogen with deuterium. In the opposite case the predominance of CH_3OD would be the result of an exchange reaction and not of the synthesis.

Perhaps the most powerful mechanistic tool is the *trapping of intermediates* by reactive chemicals. For example, dimethyl- and diethylsulfate were used for trapping of surface methoxides and formates (*86*). Unsaturated

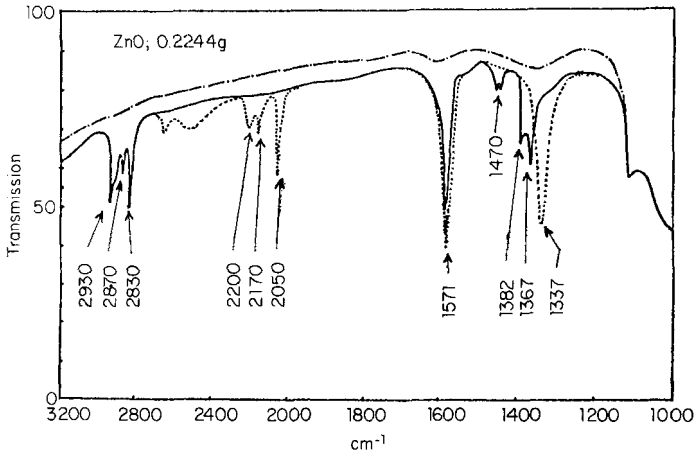

FIG. 24. Infrared spectra of methanol chemisorbed on zinc oxide at 200°C: (·—·) background; (—) CH_3OH; (···) CD_3OD. The bands at 2930 and 2830 cm^{-1} are assigned to the CH_3 asymmetric and symmetric stretching vibrations of surface methoxide ions. Bands at 2870, 1571, and 1367 cm^{-1} are assigned to the C—H stretching, O—C—O antisymmetric stretching, and O—C—O symmetric stretching vibrations of surface formate ions. Further details of assignments are given in Ref. *88*. [Reprinted with permission from *Trans. Faraday Soc.* **67**, 3585 (1971). Copyright (1971) Chemical Society, London.]

hydrocarbons and heteroatomic compounds may be considered for trapping of hydroxycarbenes as illustrated by the many examples given by E. O. Fischer (*87*). In methanol synthesis, however, most of the unsaturated compounds will undergo a competitive hydrogenation (*63*), and their reactions with the fleeting intermediates may not be readily observable.

Finally, if conditions can be found under which the kinetically significant intermediates appear in sufficiently large surface concentrations, various *surface spectroscopic methods* may be used for their detection. As an example, IR spectra of surface methoxide and formate are shown in Fig. 24 (*88*). Spectra of surface hydroxyls and hydrides (*89–92*), as well as of alkyl groups (*93*), carbonates, and carbonyls (*94*) have been well described. The vibrational spectra on small flat surfaces can also be determined by electron energy-loss spectroscopy (EELS). Semiquantitative surface analysis can be obtained from Auger electron (AES) or X-ray photoelectron (XPS) spectroscopy. Information on which orbitals of the adsorbed reactants, intermediates, and products are involved in bonding with the catalyst surface may be gained from an analysis of UV photoelectron spectroscopic (UPS) data. All of the methods cited in this section have been used with varying degrees of success for the detection of intermediates in methanol synthesis and decomposition. Additional mechanistic conclusions have been made on the basis of the change of product composition or of reaction rate upon a deliberate modification of the catalyst by bulk or surface dopants, and from analogies with the chemical behavior of metal–organic complexes.

C. Evidence for Adsorbed Carbon Monoxide and Hydrogen

Hydrogen is weakly adsorbed on copper metal, on zinc oxide, and on the copper–zinc oxide catalysts (*43*). However, a variable portion of the adsorbate is irreversibly bound. On zinc oxide, IR bands at 3400–3500 and 1475–1708 cm^{-1} were attributed to the stretching vibrations of OH and ZnH groups, respectively, and various workers agree that the OH and ZnH groups originate from heteropolar dissociation of hydrogen molecules on adjacent zinc and oxygen surface sites (*89–92*). Hydrogen chemisorption on copper is nondissociative at temperatures below 300°C because the H_2/D_2 conversion does not occur at these conditions (*95*).

Carbon monoxide adsorption on ZnO has been found to depend strongly on the pretreatment of the oxide. Kortüm and Knehr (*94*) detected a weakly bound CO with at least one rotational degree of freedom showing rotational–vibrational bands with maxima at 2188 and 2120 cm^{-1} and a strongly bound complex similar to bidentate carbonate. In addition, well-degassed ZnO specimens adsorbed CO with the IR frequency within the carbonyl

range, 1800–2100 cm^{-1}. The sites for this carbonyl-type adsorbate were suggested to be interstitial Zn^{+} ions, and carbon monoxide was assumed to be bonded carbon-down in this adsorption mode. The carbonyl-like CO was highly reactive toward oxidation. No evidence for surface formate can be found in the work of Kortüm and Knehr on hydrogen-pretreated ZnO samples exposed to CO. Ostrovskii *et al.* (*96*) studied carbon monoxide adsorption on a ternary Cu/Zn/Al oxide catalyst by volumetric methods and came to the conclusion that surface carbonate was formed on oxygen-pretreated catalyst but that both the rate and the extent of CO adsorption were low on oxygen-depleted catalyst.

The chemisorption studies of Parris and Klier (*43*) using the Cu/ZnO catalyst have been mentioned earlier. Carbon monoxide was irreversibly bonded at room temperature to the surface of the binary catalysts that were also active in methanol synthesis; however, this irreversible adsorbate could be desorbed as CO, which indicates that it was not a surface carbonate but rather a strongly bonded carbonyl-type CO. Infrared studies of this chemisorbate are lacking and it would be very desirable to determine the structure of this surface species.

Carbon monoxide chemisorption on copper metal is weak and for the most part reversible, and has been studied by a number of techniques (*97–103*).

D. Evidence for Adsorbed Formate and Methoxide

Surface formate and methoxide bands have been detected by IR spectroscopy in methanol decomposition over zinc oxide (*88*) and in the shift reaction over the Cu/ZnO catalyst (*104*). The surface methoxide, which is characterized by the CH symmetric stretch at 2840 cm^{-1} specific for the CH_3O group, was also detected in IR spectra of methanol chemisorbed on iron, nickel, and cobalt (*105*), magnesia (*106*), and alumina (*107–112*). Bowker and Madix (*82*) used UPS, XPS, and thermal desorption techniques to identify products of methanol adsorption on the Cu(110) crystal face and determined that methanol orbitals which have the highest electron density on the oxygen atom were most affected by bonding to the surface. Their findings are consistent with half monolayer coverage of methoxy species originating from methanol dissociation on the clean Cu(110) surface at 270 K. It is evident that surface methoxide is a fairly common product of the interaction of methanol with solids which are methanol catalysts as well as with many other solids that are not catalysts for methanol. To provide complete information, however, the fate of hydrogen from the methanol hydroxyl should also be determined. This hydrogen is expected to end up

in an M—H bond on metals and in an O—H bond on oxides. The M—H and O—H stretching vibrations, so far unreported in methanol decomposition studies, should be readily detectable in IR spectra.

Methoxide and formate were also found by chemical trapping with $SO_4(CH_3)_2$ and $SO_4(C_2H_5)_2$ of surface complexes formed in methanol synthesis over the BASF ZnO/Cr_2O_3 catalyst (*86*) according to the reactions

$$R_2SO_4 + 2CH_3O^- \rightarrow 2CH_3OR + SO_4^{2-} \quad (17)$$

$$R_2SO_4 + 2HCOO^- \rightarrow 2HCOOR + SO_4^{2-} \quad (18)$$

where R is methyl or ethyl. Both the methoxide and the formate were found when the synthesis was run in a flow system at 250°C, 50 atm, and $H_2/CO = 2$, with the $CH_3O^-/HCOO^-$ ratio being equal to 7.9; 0.5% of methyl formate was also detected in the methanol product.

E. Surface Complexes Formed by Coadsorption of the Reactants

Many studies of simultaneous adsorption of hydrogen or water and CO or CO_2 have been carried out on the high-pressure methanol synthesis catalysts based on zinc oxide and one or several other oxides, but only three investigations (*104*, *113*, *114*) dealt with catalysts containing copper, and two of these were made in reference to the mechanism of the low-temperature shift reaction.

The interaction of adsorbed *carbon monoxide and hydrogen* was examined by IR spectroscopy and other methods. A mutual enhancement of CO and H_2 adsorption on zinc oxide was reported in an early study by Nagarjunan *et al.* (*115*) to occur at 0 and 25°C and interpreted as the formation of the complex =CHOH, i.e., hydroxycarbene, in the adsorbed phase. However, a more recent IR investigation of Boccuzzi *et al.* (*116*) provided evidence for interaction of adsorbed carbon monoxide and hydrogen of a different kind than attributable to the formation of hydroxycarbene. At room temperature, carbon monoxide admitted to zinc oxide with preadsorbed hydrogen was found to perturb both the Zn—H (1700 cm^{-1}) and O—H (3520 cm^{-1}) bands originating from hydrogen chemisorption. While the OH frequencies were shifted upward, new discrete lower frequency bands of ZnH at 1680–1690 and 1660–1670 cm^{-1} were formed, the relative intensities of which depended on CO pressure, as illustrated in Fig. 25. These new bands cannot be assigned to any expected bands of hydroxycarbene. The carbon monoxide adsorption was accompanied by a carbonyl-type band at 2180 cm^{-1} and was attributed to carbon-down species on the cations since it was displaceable by pyridine. A model explaining the more pronounced effect of CO on

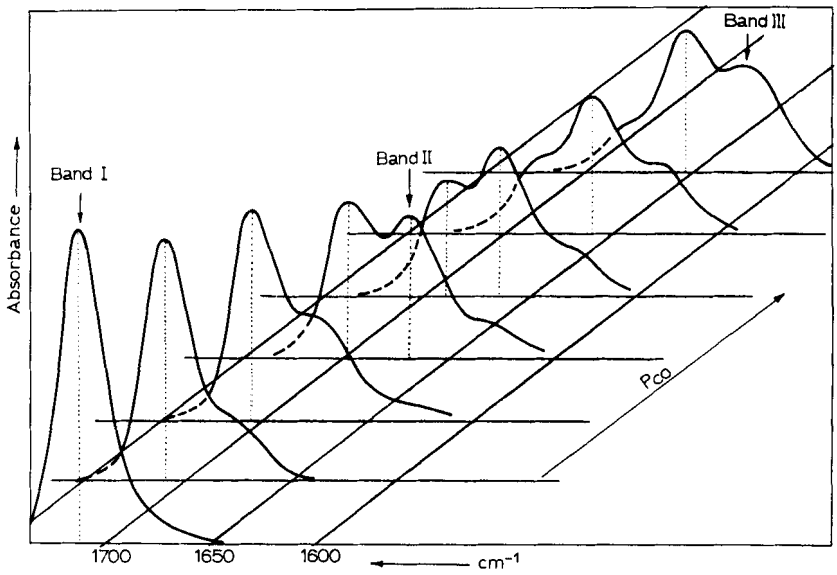

FIG. 25. Effect of increasing CO pressure on the Zn—H stretching bands on zinc oxide (P_{H_2} = 100 Torr) (*116*). [Reprinted with permission from *J. Catal.* **51,** 160 (1978). Copyright (1978) Academic Press, New York.]

the ZnH and less pronounced effect on the OH band, proposed by Boccuzzi *et al.* (*116*), is illustrated in Fig. 26. No IR bands of surface formates, methoxides, or carbonates appeared in the spectra of ZnO with hydrogen and CO coadsorbed at room temperature. More surprisingly, no surface complexes were detected upon coadsorption of CO and H_2 at temperatures

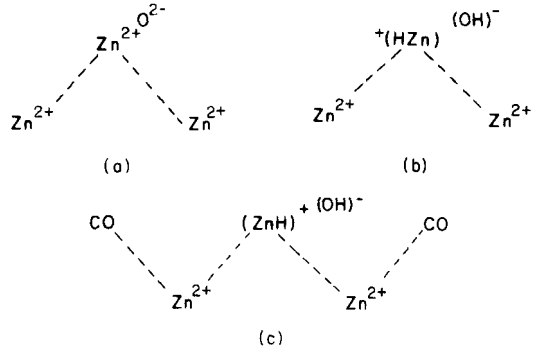

FIG. 26. Model for coadsorption of carbon monoxide and hydrogen explaining the infrared shifts in Fig. 25 (*116*): (a) clean surface; (b) hydrogen-covered surface; (c) hydrogen- and carbon monoxide-covered surface. [Reprinted with permission from *J. Catal.* **51,** 160 (1978). Copyright (1978) Academic Press, New York.]

up to 300°C and pressures of 1 Torr followed by programmed thermal desorption in the study of Bowker *et al.* (*84*). These authors concluded that no stable surface formate is formed on ZnO from carbon monoxide and hydrogen, and their conclusion must be held valid within the temperature and pressure range outlined above. However, Deluzarche *et al.* (*86*) employed pressures up to 50 atm at 250°C and were able to trap chemically both surface formate and methoxide when a ZnO/Cr_2O_3 catalyst was exposed to hydrogen and carbon monoxide either sequentially or simultaneously in the course of methanol synthesis. With an $H_2/CO = 2$ ratio in a continuous run, Deluzarche *et al.* found the ratio of surface methoxide to formate $CH_3O^-/HCOO^- = 7.9$, corresponding to an average formula $CH_{2.78}O_{1.11}$.

The amounts of coadsorbed carbon monoxide and hydrogen were also measured during methanol synthesis over the $Cu/ZnO/Cr_2O_3$ catalysts (*114*) at atmospheric pressure and 250°C with a widely varying ratio of gaseous components. The adsorption of each reactant was enhanced in the presence of the other. The principal result of this study is represented in Fig. 27. The authors noted that the average composition of the adsorbate, $H_2:CO = 1.5:1$, corresponded to the stoichiometric formula CH_3O and concluded that the synthesis rate is limited by the hydrogenation of this complex. A closer inspection of Fig. 27 indicates that the $H_2:CO$ ratio on the surface varied from 1:1 to 2:1 as the gaseous concentration of hydrogen increased, corresponding to stoichiometric formulas CH_2O to CH_3OH. Thus several intermediates may be responsible for the mutual enhancement of the carbon monoxide and hydrogen adsorption during the synthesis.

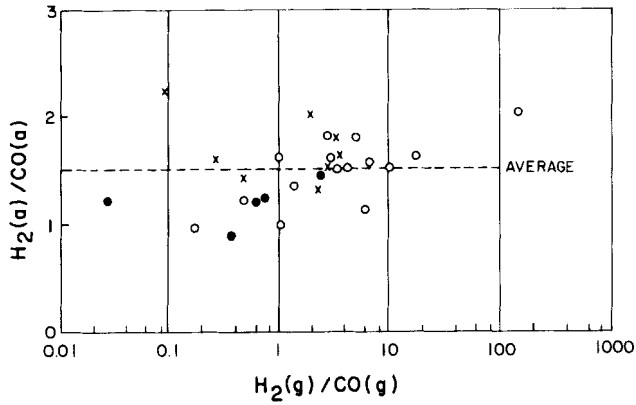

FIG. 27. Relationship between $H_2(g)/CO(g)$ and $H_2(a)/CO(a)$, the ratios of hydrogen and carbon monoxide concentrations in the gas (g) and adsorbed (a) phase during methanol synthesis (○ and ●) and decomposition (×) over $Cu/ZnO/Cr_2O_3$ catalyst at 250°C (*114*). [Reprinted with permission from *Bull. Chem. Soc. Jpn.* **38,** 1727 (1965). Copyright (1965) Chemical Society, Japan.]

Kinetic evidence for synergic adsorption of *carbon monoxide and water* on the low-temperature shift catalyst $Cu/ZnO/Fe_2O_3$ was obtained by van Herwijnen and deJong (*113*), and IR spectra of surface formate were detected on several oxide catalysts, including CuO/MgO, at temperatures as low as 20°C and pressures of 20 Torr, as reported by Davydov *et al.* (*104*). Decomposition of the surface formate to CO_2 and H_2 occurred at 100–150°C over the Cu/MgO catalyst and at 250–300°C over the MgO catalyst, and the promotion effect of copper was attributed to the formation and decomposition of a labile surface formate $(HCOO)_2Cu$. Ueno *et al.* (*117*) have shown earlier that surface formates are formed on zinc oxide, from CO and H_2O as well as from CO_2 and H_2, and hence an associative mechanism of the shift and reverse-shift reaction, involving formate intermediate, is believed to operate on many oxide catalysts.

Carbon dioxide and hydrogen also interact with the formation of surface formate. This was documented for ZnO by the IR investigation of Ueno *et al.* (*117*) and, less directly, by coadsorption-thermal decomposition study (*84*). Surface complex was formed from CO_2 with H_2 at temperatures above 180°C, which decomposed at 300°C with the evolution of carbon monoxide and hydrogen at the ratio $CO:H \cong 1:1$. When carbon dioxide and hydrogen were adsorbed separately, the CO_2 and H_2 desorption temperatures were different, indicating conclusively that a surface complex was formed from CO_2 and H_2. A complex with the same decomposition temperature was obtained upon adsorption of formaldehyde and methanol. Based upon the observed stoichiometry of decomposition products and upon earlier reported IR spectra of $CO_2 + H_2$ coadsorbates, this complex was identified as surface formate. Table XVI compares the thermal decomposition peak temperatures and activation energies, product composition, and surface

TABLE XVI

Adsorbed Species, Coverages, and Desorption Activation Energies[a]

Adsorbed species	Major TPRS products	Peak temperature (K)	E_d^b (kJ mol^{-1})	Maximum total coverage observed (cm^2)
CO_2	CO_2	390, 420, 510, 560	109, 117, 142, 153	10^{13}
H	H_2	420, 465, 540	117, 130, 150	6×10^{12}
Formate				
$CO_2 + H_2$	CO, H_2	~570	~157	3×10^{13}
H_2CO	CO, H_2	580	160	10^{14}
CH_3OH	CO, H_2	580	160	10^{14}

[a] From Ref. *84*.

[b] Calculated assuming a preexponential factor of 10^{13} sec^{-1}.

coverage for the surface formate from $CO_2 + H_2$, formaldehyde, and methanol with the desorption temperatures for carbon dioxide and hydrogen.

The coadsorption and IR spectroscopic studies cited in this section indicate that surface formate is readily formed from CO_2 and H_2 or from CO and H_2O vapors. It appears that the reaction of CO and H_2 to formate is considerably more difficult. Moreover, while both formate and methoxide have been detected in methanol decomposition over ZnO and in the synthesis over the ZnO/Cr_2O_3 catalysts, no positive evidence of these species has so far been gathered for the copper-based catalysts.

F. Mechanism of Methanol Synthesis at Low Temperatures and Pressures

It has been shown conclusively that methanol can be decomposed over various catalysts to carbon monoxide and hydrogen via surface methoxide and formate, and therefore a reversed path must exist for the synthesis. This has been confirmed by the trapping experiments that detected formate and methoxide during methanol synthesis. However, there persists the principal question whether more effective mechanisms may operate at low temperatures and pressures. Since the associative formate mechanism of the synthesis from carbon monoxide requires a source of oxygen additional to that of CO, be it water, surface OH groups, or CO_2 through the reverse-shift reaction, isotopic labeling of the feed gas may provide a clue to the mechanism: if methanol from a mixture of $^{13}C^{16}O$ and $^{12}C^{8}O$ contains only unscrambled molecules $^{13}CH_3{}^{16}OH$ and $^{12}CH_3{}^{18}OH$, the formate mechanism and any other mechanism leading to isotope exchange

$$R^{13}C^{18}O + R^{12}C^{16}O \rightleftharpoons R^{12}C^{18}O + R^{13}C^{16}O$$

where R is any substituent including the catalyst oxygen, must be ruled out. Such an experiment has in fact been performed with the use of the Rh/TiO_2 catalyst (*118*), and only isotopically unscrambled methanol molecules have been found. Thus there is evidence, at least on one catalyst, for a synthesis mechanism that does not proceed via surface formate. Bowker *et al.* (*84*) also proposed a low-temperature mechanism, as a minor pathway in addition to the formate mechanism, wherein carbon monoxide and hydrogen react via formyl, formaldehyde, and methoxide to methanol over zinc oxide.

The current mechanistic findings and interpretations are summarized in Fig. 28. Evidence for all pathways indicated in Fig. 28 exists but the reaction conditions and catalysts differ. It is likely that palladium, platinum, and

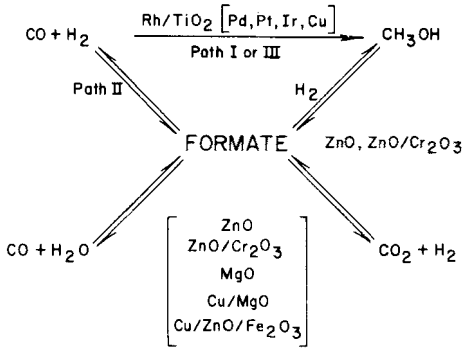

FIG. 28

iridium and copper metal will behave similarly as the Rh/TiO_2 catalyst, and therefore they were assigned the pathway bypassing the formate intermediate. It is not known at the present time whether methanol synthesis over the Cu/ZnO catalysts runs the course similar to that over the precious-metal catalyst or over the ZnO catalysts. In the latter case the specificity of the promotion effect of copper would require an explanation analogous to that proposed for the function of the CuO/MgO-shift catalyst, namely that ionic state of copper in the oxide matrix accelerates not only the decomposition but also hydrogenation of the surface formate. The specific composition of surface intermediates on the Cu/ZnO catalysts has yet to be determined. A mechanism involving carbon-down CO and formyl, which flips over to be hydrogenated to methoxide and methanol, has been proposed by Kung (*119*) and by Bowker *et al.* (*84*) for the low-temperature synthesis on ZnO. This mechanism would also bypass the formate route and involves a crossing of pathway I into pathway II prior to methanol formation.

Further mechanistic probing into the synthesis pathways over the copper-based catalysts appears very desirable. In particular, trapping, isotope, and spectroscopic studies may reveal further mechanistic details. It is important to conduct such investigations under the synthesis conditions, since at other conditions intermediates irrelevant to the synthesis may become prominent. Despite our limited knowledge of the mechanism, however, significant progress has been made in the characterization of the active component of the copper-based catalysts, in the modeling of the CO/CO_2 dependence of the synthesis rate, based on sound mechanistic features, and in the understanding of the physicochemical concepts according to which selective methanol catalysts may be chosen and further developed.

References

1. Patart, M., French Patent 540,343 (Aug. 1921).
2. Audibert, E., and Raineau, A., *Ind. Eng. Chem.* **20,** 1105 (1928).
3. Sabatier, P., and Senderens, J. B., *Ann. Chim. Phys.* **4,** 418 (1905).
4. Sabatier, P., and Mailhe, A., *C. R.* **146,** 1376 (1908).
5. Lormand, C., *Ind. Eng. Chem.* **17,** 430 (1925).
6. Frolich Per, K., Fenske, M. R., and Quiggle, D., *Ind. Eng. Chem.* **20,** 694 (1928).
7. Frolich Per, K., Fenske, M. R., Taylor, P. S., and Southwich, C. A., Jr., *Ind. Eng. Chem.* **20,** 1327 (1928).
8. Frolich Per, K., Davidson, R. L., and Fenske, M. R., *Ind. Eng. Chem.* **21,** 109 (1929).
9. Kostelitz, O., and Hüttig, G. F., *Kolloid Z.* **67,** 265 (1934).
10. Natta, G., *Catalysis* **3,** 349 (1955).
11. Bröcker, F. J., Marosi, L., Schröder, W., and Schwarzmann, M., German Patent 2,056,612 (May 31, 1972); assigned to Badische Anilin- & Soda-Fabrik AG.
12. Catalysts and Chemicals, Inc., German Patent 1,965,007 (Oct. 15, 1970).
13. Collins, B. M., German Patent 2,302,658 (Aug. 2, 1973); assigned to Imperial Chemical Ind., Ltd.
14. Shishkov, D. S., and Kasabova, N. A., *Dokl. Bulg. Akad. Nauk* **27,** 73 (1974).
15. French Patent 1,489,682 (July 21, 1967); assigned to Imperial Chemical Ind., Ltd.
16. French Patent 2,037,567 (Dec. 21, 1970); assigned to Imperial Chemical Ind., Ltd.
17. Kotera, Y., Oba, M., Ogawa, K., Shimomura, K., and Uchida, H., *in* "Preparation of Catalysts" (B. Delmon, P. A. Jacobs, and G. Poncelet, eds.), pp. 489–597. Elsevier, Amsterdam, 1976.
18. Stiles, A. B., German Patent 2,320,192 (Oct. 25, 1973); assigned to E. I. duPont de Nemours.
19. Lender, Yu. V., Tsybina, E. N., Popov, I. G., Pirozhenko, L. F., and Petrishcheva, G. S., *Khim. Prom. (Moscow)* **49,** 899 (1973).
20. Oliver, R. B., German Patent 1,229,990 (Dec. 8, 1966); assigned to Power-Gas Corp., Ltd.
21. Eguchi, T., Yamamoto, T., Yamauchi, S., Kuraishi, M., and Asakawa, K., U.S. Patent 3,256,208 (June 14, 1966); assigned to Japan Gas-Chemical Co.
22. Bröcker, F. J., German Patent 2,116,949 (Oct. 19, 1972); assigned to Badische Anilin- & Soda-Fabrik A.G.
23. Jorgensen, M. H., and Rüshede, K., German Patent 2,016,596 (Dec. 3, 1970); assigned to Topsoe, Haldor Frederik Axel.
24. Davies, P., and Snowdon, F. F., U.S. Patent 3,326,956 (June 20, 1967); assigned to Imperial Chemical Ind., Ltd.
25. Baron, G., Bechtholdt, H., Bratzler, K., Leibgolt, H., and Ehrland, E., German Patent 1,300,917 (Aug. 14, 1969); assigned to Metallgesellschaft AG.
26. Denny, P. J., and Whan, D. A., *Catalysis London* **2,** 46 (1978).
27. Andrew, S. P. S., *Post Congr. Symp. Int. Congr. Catal., 7th, Osaka,* Paper 12 (July 1980).
28. Brodén, G., Rhodin, T. N., Bruckner, C., Benbow, R., and Hurych, Z., *Surf. Sci.* **59,** 593 (1976).
29. Klier, K., Zettlemoyer, A. C., and Leidheiser, H., Jr., *J. Chem. Phys.* **52,** 589 (1970).
30. Hayward, D. O., and Trapnell, B. M. W., "Chemisorption," 2nd ed. Butterworths, London, 1964, p. 231.
31. The catalytic activity of copper metal is reviewed on pp. – .
32. Poutsma, M. L., Elek, L. F., Ibarbia, P. A., Risch, A. P., and Rabo, J. A., *J. Catal.* **52,** 151 (1978).

33. Ichikawa, M., *Bull. Chem. Soc. Jpn.* **51,** 2268 (1978).
34. Ellgen, P. C., and Bhasin, M. M., U.S. Patents 4,014,913 (March 1977); 4,096,164 (June 1978); and 4,162,262 (July 1979).
35. Early reports (1, 2) indicate that the activity of oxides follows the pattern ZnO > MnO, Cr_2O_3 > BeO, Ce_2O_3, UO_2, ZrO_2, oxides of Al, Si, Mo, W, V, Ti, Th, Mg, Ca, Ba, and Sr being inactive.
36. Klier, K., to be published (1982).
37. Bulko, J. B., Ph.D. dissertation, Lehigh University, 1980 (Univ. Microfilms Int., Order No. 8102497).
38. Bulko, J. B., Herman, R. G., and Klier, K., *J. Am. Ceram. Soc.* in press (1982).
39. Herman, R. G., Klier, K., Simmons, G. W., Finn, B. P., Bulko, J. B., and Kobylinski, T. P., *J. Catal.* **56,** 407 (1979).
40. Mehta, S., Simmons, G. W., Klier, K., and Herman, R. G., *J. Catal.* **57,** 339 (1979).
41. Bulko, J. B., Herman, R. G., Klier, K., and Simmons, G. W., *J. Phys. Chem.* **83,** 3118 (1979).
42. Parris, G. E., Ph.D. Dissertation, Lehigh University, 1981.
43. Parris, G. E., and Klier, K., to be published (1982).
44. Chapple, F. H., and Stone, F. S., *Proc. Br. Ceram. Soc.* **1,** 45 (1964).
45. Schiavello, M., Pepe, F., and DeRossi, S., *J. Phys. Chem.* **92,** 109 (1974).
46. Kochloefl, K., *Proc. Int. Congr. Catal., 7th, Tokyo 1980* p. 486 (1981).
47. Notari, B., discussion to paper A 32, *Proc. Int. Congr. Catal., 7th, Tokyo 1980* p. 487 (1981).
48. Zettlemoyer, A. C., Yu, Y. F., Chessick, J. J., and Healey, F. H., *J. Phys. Chem.* **61,** 1319 (1957).
49. Kington, G. L., and Holmes, J. M., *Trans. Faraday Soc.* **49,** 425 (1953).
50. Vasilevich, A. A., Shpiro, G. P., Alekseev, A. M., Semenova, T. A., Markina, M. I., Vasil'eva, T. A., and Budkina, O. G., *Kinet. Catal.* (English ed.) **16**(6), 1363 (1975).
51. Yao, Y.-F. Y., *J. Phys. Chem.* **69,** 3930 (1965).
52. Kummer, J. T., and Yao, Y.-F. Y., *Can. J. Chem.* **45,** 421 (1967).
53. Sherwin, M., and Blum, D., "Liquid Phase Methanol." Report to the Electric Power Research Inst., EPRI AF-202, Research Project 317-1 (August 1976).
54. Simmons, G. W. *et al.*, to be published.
55. Chatikavanij, V., M. S. Thesis, Lehigh University, 1980.
56. Klier, K., Chatikavanij, V., Herman, R. G., and Simmons, G. W., *J. Catal.* **74,** 343 (1982).
57. Natta, G., Pino, P., Mazzanti, G., and Pasquon, I., *Chim. Ind.* **35,** 705 (1953).
58. Pasquon, I., and Dente, M., *J. Catal.* **1,** 108 (1962).
59. Wermann, J., Lukas, K., and Gelbin, D., *Z. Phys. Chem.* **225,** 234 (1964).
60. Bakemeier, H., Laurer, P. R., and Schroder, W., *Chem. Eng. Prog. Symp. Ser.* **66**(98), 1 (1970).
61. Leonov, V. E., Karavaev, M. M., Tsybina, E. N., and Petrishcheva, G. S., *Kinet. Catal.* (English ed.) **14,** 848 (1973).
62. van Herwijnen, T., and deJong, W. A., *J. Catal.* **34,** 209 (1974).
63. Vedage, G., and Klier, K., *J. Catal.* in press (1982).
64. Vannice, M. A., *J. Catal.* **37,** 449 (1975); reports turnover rate of 3.2×10^{-2} sec^{-1} at 275°C for hydrogenation of CO to methane over nickel catalysts, while turnover rate for benzene hydrogenation can be estimated at 0.77×10^{-7} sec^{-1} at 66°C and a minimum of 0.46 sec^{-1} at 275°C from data given in the report by Danes, V., Cabicar, J., Grubner, O., Klier, K., and Jiru, P., *Chem. Listy* **50,** 1049 (1956); see also Ref. *63*.
65. Cotton, F. A., and Marks, T. J., *J. Am. Chem. Soc.* **92,** 5114 (1970).
66. Herberhold, M., "Metal π-Complexes," pp. 227–232. Elsevier, Amsterdam, 1972.

67. Cotton, F. A., and Wilkinson, G., "Advanced Inorganic Chemistry," 3rd ed. Wiley, New York, 1972.
68. Baglin, E. G., Atkinson, G. B., and Nicks, L. J., *Ind. Eng. Chem.* **20,** 87 (1981).
69. Scholten, J. F. F., and Konvalinka, J. A., *Trans. Faraday Soc.* **65,** 2465 (1969).
70. Ponec, V., *Proc. Int. Congr. Catal., 7th, Tokyo 1980* p. 486 (1981).
71. Ichikawa, M., *Bull. Chem. Soc. Jpn.* **51,** 2273 (1978).
72. Ichikawa, M., and Shikakura, K., *Proc. Int. Congr. Catal., 7th, Tokyo 1980* pp. 925–940 (1981).
73. Klier, K., and Herman, R. G., unpublished results.
74. Ellgen, P. C., Bartley, W. J., Bhasin, M. M., and Wilson, T. P., *Adv. Chem.* **178,** 147 (1979).
75. Klier, K., *Proc. Conf. Catal. Organ. Synth., 8th* pp. 75–89 (1981).
76. Fischer, A., Hosemann, R., Vogel, W., Koutecký, J., Pohl, J., and Rálek, M., *Proc. Int. Congr. Catal., 7th, Tokyo 1980* p. 341 (1981).
77. Herman, R. G., Simmons, G. W., and Klier, K., *Proc. Int. Congr. Catal., 7th, Tokyo 1980* p. 475 (1981).
78. Sugier, A., and Freund, E., U.S. Patent 4,122,110 (Oct. 1978).
79. Sugier, A., and Freund, E., Fr. Patent 2,369,234 (May 1978).
80. Sugier, A., and Freund, E., Ger. Offen. 2,748,097 (May 1978).
81. Wachs, I. E., and Madix, R. J., *J. Catal.* **53,** 208 (1978).
82. Bowker, M., and Madix, R. J., *Surf. Sci.* **95,** 190 (1980).
83. Madix, R. J., *Adv. Catal.* **29,** 1 (1980).
84. Bowker, M., Houghton, H., and Waugh, K. C., *J. Chem. Soc. Faraday Trans. I,* **77,** 3023 (1981).
85. Borowitz, J. L., *J. Catal.* **13,** 106 (1969).
86. Deluzarche, A., Kieffer, R., and Muth, A., *Tetrahedron Lett.* **38,** 3357 (1977).
87. Fischer, E. O., *Adv. Organomet. Chem.* **14,** 1 (1976).
88. Ueno, A., Onishi, T., and Tamaru, K., *Trans. Faraday Soc.* **67,** 3585 (1971).
89. Eischens, R. P., Pliskin, W. A., and Low, M. J. D., *J. Catal.* **1,** 180 (1962).
90. Chang, C. C., Dixon, L. T., and Kokes, R. J., *J. Phys. Chem.* **77,** 2634 (1973).
91. Dent, A. L., and Kokes, R. J., *J. Phys. Chem.* **73,** 3772 (1969).
92. Boccuzzi, F., Borello, E., Zecchina, A., Bossi, A., and Camia, M., *J. Catal.* **51,** 150 (1978).
93. Carrizosa, I., Munuera, G., and Castañar, S., *J. Catal.* **49,** 265 (1977).
94. Kortüm, G., and Knehr, H., *Z. Phys. Chem. N.F.* **89,** 194 (1974).
95. Mikovsky, R. J., Boudart, M., and Taylor, H. S., *J. Am. Chem. Soc.* **76,** 3814 (1954).
96. Ostrovskii, V. E., Dyatlov, A. A., and Ogneva, T. P., *Kinet. Catal.* (English ed.) **19,** 410 (1978).
97. Tracy, J. C., *J. Chem. Phys.* **56,** 2748 (1972).
98. Pritchard, J., Catterick, T., and Gupta, R. K., *Surf. Sci.* **53,** 1 (1975).
99. Doyen, G., and Ertl, G., *Surf. Sci.* **43,** 197 (1974).
100. Papp, H., and Pritchard, J., *Surf. Sci.* **53,** 371 (1975).
101. Alexander, C. S., and Pritchard, J., *J. Chem. Soc. Faraday Trans. I,* **68,** 202 (1972).
102. Thurston, E. F. W., *Trans. Faraday Soc.* **64,** 2181 (1968).
103. Smith, A. W., and Quets, J. M., *J. Catal.* **4,** 163 (1965).
104. Davydov, A. A., Boreskov, G. K., Yur'eva, T. M., and Rubene, N. A., *Dokl. Akad. Nauk USSR* **236,** 1402 (1977).
105. Blyholder, G., and Wyatt, W. V., *J. Phys. Chem.* **70,** 1745 (1966).
106. Kagel, R. O., and Greenler, R. G., *J. Chem. Phys.* **49,** 1638 (1968).
107. Soma, Y., Onishi, T., and Tamaru, K., *Trans. Faraday Soc.* **65,** 2215 (1969); Greenler, R. G., *J. Chem. Phys.* **37,** 2094 (1962).

108. Treibmann, D., and Simon, A., *Ber. Bunsenges. Phys. Chem.* **70,** 562 (1966).
109. Arai, H., Take, J., Saito, Y., and Yoneda, Y., *J. Catal.* **9,** 146 (1967).
110. Kagel, R. O., *J. Phys. Chem.* **71,** 844 (1967).
111. Deo, A. V., and Dalla Lana, I. G., *J. Phys. Chem.* **73,** 716 (1969).
112. Hertl, W., and Guenca, A. M., *J. Phys. Chem.* **77,** 1120 (1973).
113. Herwijnen, T., van, and deJong, W. A., *J. Catal.* **63,** 83 (1980).
114. Tsuchiya, S., and Shiba, T., *Bull. Chem. Soc. Jpn.* **38,** 1726 (1965).
115. Nagarjunan, T. S., Sastri, M. V. C., and Kuriacose, J. C., *J. Catal.* **2,** 223 (1963).
116. Boccuzzi, F., Garrone, E., Zecchina, A., Bossi, A., and Camia, M., *J. Catal.* **51,** 160 (1978).
117. Ueno, A., Onishi, T., and Tamaru, K., *Trans. Faraday Soc.* **66,** 756 (1970).
118. Takeuchi, A., and Katzer, J. R., *J. Phys. Chem.* **85,** 937 (1981).
119. Kung, H. H., *Catal. Rev.* **22,** 235 (1980).